A High-Valent Nonheme Iron Intermediate. Structure and Properties of $[Fe_2(\mu\text{-}O)_2(5\text{-Me-TPA})_2](ClO_4)_3$

Yanhong Dong,[†] Hiroshi Fujii,[†] Michael P. Hendrich,[†] Randolph A. Leising,[†] Gaofeng Pan,[†] Clayton R. Randall,[†] Elizabeth C. Wilkinson,[†] Yan Zang,[†] Lawrence Que, Jr.,*[,†] Brian G. Fox,[‡] Karl Kauffmann,[‡] and Eckard Münck*[,‡]

Contribution from the Departments of Chemistry, University of Minnesota, Minneapolis, Minnesota 55455, and Carnegie Mellon University, Pittsburgh, Pennsylvania 15213

Received September 19, 1994[⊗]

Abstract: In our efforts to model the oxygen activation chemistry of methane monooxygenase (MMO) and the R2 protein of ribonucleotide reductase (RNR), we have discovered a transient green species (**3**) in the reaction of H_2O_2 with a (μ-oxo)diiron(III) TPA complex (TPA = tris(2-pyridylmethyl)amine). Our studies show that the precursor to **3** is $[Fe_2O(TPA)_2(OH)(H_2O)](ClO_4)_3$ (**2a**), which can be obtained by the treatment of $[Fe_2O(TPA)_2(H_2O)(ClO_4)](ClO_4)_3$ (**1**) with an equivalent of base. Crystallographic studies show that **1** has a nearly linear (μ-oxo)diiron(III) core with terminal aqua and perchlorato ligands ($\angle$Fe−(μ-O)−Fe = 174.1(4)°), while **2c**, the 5-Et-TPA analogue of **2a**, has a bent (μ-oxo)diiron(III) core that is supported by an $H_3O_2^-$ bridge. The presence of an $H_3O_2^-$ bridge in the latter is indicated by the short O−O separation (2.464(9) Å), the Fe−Fe distance of 3.346(9) Å, and the Fe−(μ-O)−Fe angle of 136.3(3)°. Thus treatment of **1** with an equivalent of base results in the replacement of the bound perchlorate with hydroxide and the bending of the Fe−O−Fe unit to form **2**. That the bent Fe−O−Fe core persists in solution is indicated by its UV−vis features and NMR spectra that reflect distinct TPA coordination modes about the individual iron sites. The green intermediate **3** is generated by the reaction of **2**, $[Fe_2O(L)_2(OH)(H_2O)](ClO_4)_3$ (L = TPA, 5-Me-TPA, and 5-Et-TPA), with H_2O_2 in CH_3CN at −40 °C; when 5-Me-TPA is used as the tripodal ligand, **3b** can be isolated as a solid upon standing overnight at −40 °C. Complex **3b** exhibits electronic absorption features at 366 (ϵ = 7900 M^{-1} cm^{-1}) and 616 nm (ϵ = 5200 M^{-1} cm^{-1}) and an $S = {}^3/_2$ EPR spectrum with g values at 4.45, 3.90, and 2.01. It exhibits one sharp Mössbauer doublet with ΔE_Q = 0.49 mm/s and δ = 0.12 mm/s at 100 K, which accounts for 90% of the iron in the solid. Elemental analysis and electrospray ionization mass spectrometry show that **3b** is a dinuclear complex best formulated as $[Fe_2(O)_2(5\text{-Me-TPA})_2](ClO_4)_3$. This dinuclear formulation is corroborated by magnetic susceptibility measurements showing that **3b** has a high-temperature moment of 3.9 μ_B/2Fe, corresponding to the $S = {}^3/_2$ center observed by EPR. The formula for **3b** suggests two unique properties: (a) that it has an $Fe_2(\mu\text{-}O)_2$ core, and (b) that it is formally $Fe^{III}Fe^{IV}$. The presence of an $Fe_2(\mu\text{-}O)_2$ core in **3b** is indicated by its EXAFS spectrum, which requires the inclusion of an Fe scatterer at 2.89 Å for a satisfactory fit. It is further supported by the observation of resonance-enhanced Raman features at 676 and 656 cm^{-1} (both of which shift to 634 cm^{-1} with added $H_2{}^{18}O$), which are associated with an Fe_2O_2 breathing mode by analogy to those observed for Mn_2O_2 complexes. The high-valent nature of **3b** is corroborated by the ca. 3 eV upshift of its higher X-ray absorption K-edge relative to that of **2b** and the reduction of **3b** to the diiron(III) state at −40 °C by chemical (ferrocene titration) and cyclic voltammetric ($E_{1/2}$ = 0.96 V vs NHE) methods. Thus, **3b** represents a bis(μ-oxo)-diiron complex with a formally $Fe^{III}Fe^{IV}$ valence state. Complex **3b** has an unusual electronic structure. EPR, magnetization, and Mössbauer studies show that **3b** has an $S = {}^3/_2$ ground state with a large and nearly axial zero-field splitting, $D = 35 \pm 15$ cm^{-1} and E/D = 0.04. The Mössbauer data show that **3** contains two equivalent iron sites which have unusually small magnetic hyperfine interactions, **A** = (−7.8, −7.9, −6.5) MHz. A variety of exchange coupling models are considered to describe the electronic properties of **3b**; these include $Fe^{III}Fe^{III}$ sites coupled to a ligand radical and valence-delocalized $Fe^{III}Fe^{IV}$ centers. Among the models considered, the only one that could possibly explain the observed site equivalence, isomer shift, and other properties consists of a valence-delocalized low-spin ($S = {}^1/_2$) Fe^{III}−low-spin (S = 1) Fe^{IV} pair coupled by Heisenberg as well as double exchange; however, detailed theoretical studies of double exchange interactions involving low-spin iron sites are required before such an assignment can be made. Whatever its electronic structure, **3b** is the only well-characterized high-valent nonheme iron species that is derived from the reaction of H_2O_2 and a (μ-oxo)diiron(III) complex. As such, it is relevant to the transient species observed in the oxidation chemistry of MMO and RNR R2 and provides a synthetic example of how a high-valent state can be attained in a nonheme environment.

Introduction

Metalloproteins with nonheme diiron centers bridged by an oxide (or hydroxide) and carboxylates have emerged as an important class in the past decade.[1] Among the structurally characterized proteins of this class are the invertebrate dioxygen carriers hemerythrin[2] and myohemerythrin,[3] the R2 protein of the ribonucleotide reductase (RNR) from *Escherichia coli*,[4] and

[†] University of Minnesota.
[‡] Carnegie Mellon University.
[⊗] Abstract published in *Advance ACS Abstracts*, February 15, 1995.

(1) (a) Que, L., Jr.; True, A. E. *Prog. Inorg. Chem.* **1990**, *38*, 97−200. (b) Feig, A. L.; Lippard, S. J. *Chem. Rev.* **1994**, *94*, 759−805.
(2) Stenkamp, R. E. *Chem. Rev.* **1994**, *94*, 715−726.
(3) Sheriff, S.; Hendrickson, W. A.; Smith, J. L. *J. Mol. Biol.* **1987**, *197*, 273−296.

0002-7863/95/1517-2778$09.00/0 © 1995 American Chemical Society

the hydroxylase component of the methane monooxygenase (MMOH) from *Methylococcus capsulatus* (Bath).[5] Spectroscopic data place stearoyl acyl carrier protein Δ^9 desaturase,[6] rubrerythrin,[7] and the purple acid phosphatases[8] in this class as well. Amino acid sequence comparisons show the presence of recurring (D/E)XXH motifs in a subset of this group. These motifs have been found to serve as metal binding sites in the structures of RNR R2 and MMOH and are proposed to have similar functions in the active sites of the desaturase and rubrerythrin; the presence of these motifs in phenol hydroxylase[9] and toluene monooxygenase[10] has led to the suggestion[6] that these enzymes may also belong to this subset of metalloproteins.

With the exception of rubrerythrin, which has no known function, the enzymes in this subset activate dioxygen to perform their varied functions. It is clear from studies of RNR R2 and MMOH that it is the diiron(II) form that interacts with O_2 to generate the oxidizing species responsible for the oxidative transformations performed by these enzymes. Recently, spectroscopic evidence for transient oxidizing species[11-15] has been uncovered in the reactions of O_2 with the diiron(II) centers of RNR R2 and MMOH. For RNR R2, intermediates **I** and **II** are observed and found capable of oxidizing Tyr122 to its catalytically essential radical state.[11,12] Both intermediates have a diiron cluster **X** that contains one oxidizing equivalent above the diiron(III) state. Cluster **X** exhibits EPR and Mössbauer features that are associated with a coupled $S = {}^1/_2$ system consisting of two high-spin iron(III) centers and a ligand radical.[12] In the case of MMO, compounds **L** (or **P**) and **Q** have been reported;[14,15] both are kinetically competent to hydroxylate methane. Compound **L** (or **P**) is the first intermediate detected in the reaction of O_2 with $MMOH_{red}$; it then decays to compound **Q**. Based on chemical considerations and its Mössbauer properties ($\delta = 0.66$ mm/s), Liu *et al.* have proposed that compound **L** (or **P**) is a diiron(III)−peroxide species.[15] Compound **Q**, on the other hand, has significantly smaller isomer shifts ($\delta_1 = \delta_2 = 0.17$ mm/s for the MMOH from *Methylosinus trichosporium* OB3b;[13] $\delta_1 = 0.21$ mm/s and $\delta_2 = 0.14$ mm/s for the enzyme from *Methylococcus capsulatus* (Bath)[15]); the *M. trichosporium* data have been assigned to a coupled $Fe^{IV}Fe^{IV}$ species.

In our efforts to model such oxidizing species of these diiron enzymes, we observed a transient high-valent species in the reaction of a (μ-oxo)diiron(III) TPA[16] complex with H_2O_2 in CH_3CN at −40 °C.[17] This intermediate exhibits an $S = {}^3/_2$ EPR spectrum and a Mössbauer isomer shift of 0.11 mm/s, *i.e* the complex has properties very similar to those of synthetic oxoiron(IV) porphyrin radical cation species.[18] Because the initial EPR quantitations gave spin concentrations of 0.3 spin for samples that contained 30% of the iron associated with the $S = {}^3/_2$ species, we formulated the intermediate as $[Fe(TPA)O]^{3+}$; however, this mononuclear formulation has turned out to be incorrect. The use of 5-alkyl-TPA ligands in place of TPA has allowed the isolation of the high-valent species as a solid; the spectroscopic properties of the isolated solid identify it as $[Fe_2(O)_2(5\text{-R-TPA})_2](ClO_4)_3$, a bis($\mu$-oxo)diiron(III,IV) complex. We detail the spectroscopic studies in this paper.

Experimental Section

Materials and Synthesis. Reagents and solvents were purchased commercially and used as received. $H_2{}^{18}O$ (97% enriched) and D_2O (97.3% enriched) were obtained from Isotec, Inc. TPA·3$HClO_4$ was synthesized according to literature procedures.[19] Elemental analyses were performed at Galbraith Laboratories, Inc. (Knoxville, TN) and MHW Laboratories (Phoenix, AZ). *Caution! The perchlorate salts in this study are all potentially explosive and should be handled with care.*

2-(Chloromethyl)-5-methylpyridine hydrochloride was prepared according to the procedures described by Hardegger[20] and Baker et al.[21] ^1H NMR ($CDCl_3$): δ (ppm) 2.59 (s, 3H, $-CH_3$), 5.16 (s, 2H, $-CH_2Cl$), 7.96 (d, 1H), 8.24 (d, 1H), 8.56 (s, 1H).

2-(Aminomethyl)-5-methylpyridine hydrochloride. An aqueous solution of 2-(chloromethyl)-5-methylpyridine hydrochloride (3.00 g, 16.8 mmol) was neutralized with saturated Na_2CO_3 and extracted with ether. After the ether was evaporated, 2-(chloromethyl)-5-methylpyridine (1.84 g, 13.0 mmol, yield 77%) was obtained by high-vacuum distillation. A mixture of 2-(chloromethyl)-5-methylpyridine (1.84 g, 13.0 mmol) and potassium phthalimide (2.47 g, 13.3 mmol) in 13 mL of dry dimethylformamide (DMF) was warmed to 85 °C with stirring for 25 h. The mixture was cooled and treated with water (20 mL) and extracted with $CHCl_3$ (4 × 10 mL). The extract was washed with aqueous NaOH (0.15 N, 10 mL) and water (2 × 10 mL), dried over Na_2SO_4, and filtered. Solid 5-methyl-2-picolylphthalimide (2.75 g, 10.9 mmol, yield 84%) was obtained by removing $CHCl_3$. The solid then was dissolved in a mixture of 10 mL of acetic acid and 10 mL of concentrated hydrochloric acid and refluxed for 48 h during which time 3 mL of concentrated hydrochloric acid was added three times. After cooling, the mixture was filtered to remove phthalic acid, and the filtrate was concentrated to dryness under reduced pressure. The residue was treated with water, the undissolved material was filtered off, and the filtrate was again concentrated to dryness. The solid was recrystallized from MeOH and Et_2O and 1.57 g (8.05 mmol) of 2-(aminomethyl)-

(4) (a) Nordlund, P.; Sjöberg, B.-M.; Eklund, H. *Nature* **1990**, *345*, 593−598. (b) Stubbe, J. *Adv. Enzymol.* **1989**, *63*, 349−419. (c) Fontecave, M.; Nordlund, P.; Eklund, H.; Reichard, P. *Adv. Enzymol.* **1992**, *65*, 147−183.

(5) (a) Rosenzweig, A. C.; Frederick, C. A.; Lippard, S. J.; Nordlund, P. *Nature* **1993**, *366*, 537−543. (b) Lipscomb, J. D. *Annu. Rev. Microbiol.* **1994**, *48*, 371−399. (c) Green, J.; Dalton, H. *J. Biol. Chem.* **1989**, *264*, 17698−17703.

(6) Fox, B. G.; Shanklin, J.; Somerville, C.; Münck, E. *Proc. Natl. Acad. Sci. U.S.A.* **1993**, *90*, 2486−2490.

(7) Ravi, N.; Prickril, B. C.; Kurtz, D. M., Jr.; Huynh, B. H. *Biochemistry* **1993**, *32*, 8487−8491.

(8) (a) Averill, B. A.; Davis, J. C.; Burman, S.; Zirino, T.; Sanders-Loehr, J.; Loehr, T. M.; Sage, J. T.; Debrunner, P. G. *J. Am. Chem. Soc.* **1987**, *109*, 3760−3767. (b) True, A. E.; Scarrow, R. C.; Randall, C. R.; Holz, R. C.; Que, L., Jr. *J. Am. Chem. Soc.* **1993**, *115*, 4246−4255.

(9) Nordlund, I.; Powlowski, J.; Shingler, V. *J. Bacteriol.* **1990**, *172*, 6826−6833.

(10) Yen, K.-M.; Karl, M. R.; Blatt, L. M.; Simon, M. J.; Winter, R. B.; Fausset, P. R.; Lu, H. S.; Harcourt, A. A.; Chen, K. K. *J. Bacteriol.* **1991**, *173*, 5315−5327.

(11) (a) Bollinger, J. M., Jr.; Edmondson, D. E.; Huynh, B. H.; Filley, J.; Norton, J.; Stubbe, J. *Science (Washington, D.C.)* **1991**, *253*, 292−298. (b) Bollinger, J. M., Jr.; Tong, W. H.; Ravi, N.; Huynh, B.-H.; Edmondson, D. E.; Stubbe, J. *J. Am. Chem. Soc.* **1994**, *116*, 8015−8023. (c) Bollinger, J. M., Jr.; Tong, W. H.; Ravi, N.; Huynh, B. H.; Edmondson, D. E.; Stubbe, J. *J. Am. Chem. Soc.* **1994**, *116*, 8024−8032.

(12) (a) Bollinger, J. M., Jr.; Stubbe, J.; Huynh, B. H.; Edmondson, D. E. *J. Am. Chem. Soc.* **1991**, *113*, 6289−6291. (b) Ravi, N.; Bollinger, J. M., Jr.; Huynh, B. H.; Edmondson, D. E.; Stubbe, J. *J. Am. Chem. Soc.* **1994**, *116*, 8007−8014.

(13) Lee, S.-K.; Fox, B. G.; Froland, W. A.; Lipscomb, J. D.; Münck, E. *J. Am. Chem. Soc.* **1993**, *115*, 6450−6451.

(14) Lee, S.-K.; Nesheim, J. C.; Lipscomb, J. D. *J. Biol. Chem.* **1993**, *268*, 21569−21577.

(15) Liu, K. E.; Wang, D.; Huynh, B. H.; Edmondson, D. E.; Salifoglou, A.; Lippard, S. J. *J. Am. Chem. Soc.* **1994**, *116*, 7465−7466.

(16) Abbreviations used: Hacac = 2,4-pentanedione; H_2Pc = phthalocyanine; H_2salen = *N,N'*-ethylenebis(salicylideneamine); H_2sal_2trien = Schiff base adduct of salicylaldehyde and triethylenetetramine; 5-Et-TPA = tris(5-ethyl-2-pyridylmethyl)amine; tmima = tris((1-methylimidazol-2-yl)methyl)amine; 5-Me-TPA = tris(5-methyl-2-pyridylmethyl)amine; 6-Me-TPA = tris(6-methyl-2-pyridylmethyl)amine; $H_2T(2\text{-N-Me})PyP$ = tetrakis(2-*N*-methylpyridiniumyl)porphin tetracation; TPA = tris(2-pyridylmethyl)amine; H_2TPP = tetraphenylporphin.

(17) Leising, R. A.; Brennan, B. A.; Que, L., Jr.; Fox, B. G.; Münck, E. *J. Am. Chem. Soc.* **1991**, *113*, 3988−3990.

(18) Mandon, D.; Weiss, R.; Jayaraj, K.; Gold, A.; Temer, J.; Bill, E.; Trautwein, A. X. *Inorg. Chem.* **1992**, *31*, 4404−4409.

(19) (a) Anderegg, G.; Wenk, F. *Helv. Chim. Acta* **1967**, *50*, 2330−2332. (b) Gafford, B. G.; Holwerda, R. A. *Inorg. Chem.* **1989**, *28*, 60−66.

(20) Hardegger, E.; Nikles, E. *Helv. Chim. Acta* **1957**, *40*, 2428−2433.

(21) Baker, W.; Buggle, K. M.; McOmie, J. F. W.; Watkins, D. A. M. *J. Chem. Soc. (London)* **1958**, 3594−3603.

5-methylpyridine hydrochloride (yield 74%) was obtained. ^{1}H NMR (D_2O): δ (ppm) 2.33 (s, 3H, $-CH_3$), 4.34 (s, 2H, $-CH_2NH_2$), 7.71 (d, 1H), 8.15 (d, 1H), 8.45 (s, 1H).

Tris(5-methyl-2-pyridylmethyl)amine (5-Me-TPA). A mixture of 1.57 g (8.05 mmol) of 2-(aminomethyl)-5-methylpyridine hydrochloride and 2.87 g (16.1 mmol) of 2-(chloromethyl)-5-methylpyridine hydrochloride in 10 mL of water was neutralized with NaOH (1.93 g, 49.3 mmol) in 4 mL of water at 0 °C. This solution was stirred at room temperature for 3 days, and the white solid product (2.22 g, 6.68 mmol) precipitated in 83% yield. ^{1}H NMR ($CDCl_3$): δ (ppm) 2.29 (s, 3H, $-CH_3$), 3.81 (s, 2H, $-CH_2N$), 7.46 (s, 2H), 8.38 (s, 1H).

Tris(5-ethyl-2-pyridylmethyl)ammonium perchlorate (5-Et-TPA · $3HClO_4$) was prepared from 2-methyl-5-ethylpyridine by the procedures similar to those described for 5-Me-TPA except that $HClO_4$ was used in order to obtain solid ligand. ^{1}H NMR (D_2O): δ (ppm) 1.06 (t, 3H, $-CH_2CH_3$), 2.62 (m, 2H, $-CH_2CH_3$), 4.13 (s, 2H, $-CH_2N$), 7.71 (d, 1H), 8.14 (d, 1H), 8.36 (s, 1H).

$[Fe_2O(TPA)_2(H_2O)(ClO_4)](ClO_4)_3$ (1) was prepared by mixing TPA · $3HClO_4$ (0.404 g, 0.682 mmol) and Et_3N (0.276 g, 2.73 mmol) in 10 mL of methanol and $Fe(ClO_4)_3 \cdot 10H_2O$ (0.364 g, 0.682 mmol) in 2 mL of methanol. The resulting red/brown solution was concentrated down to approximately 4 mL and then placed in the freezer. Red crystalline material was isolated the next day: ^{1}H NMR (CD_3CN, −40 °C): δ (ppm) 46.8 and 28.7 (br, α-pyr or CH_2), 18.1 (β-pyr), 8.1 (br, CH_2), 6.2 and 5.9 (γ-pyr). Anal. Calcd for $[Fe_2O(TPA)_2(H_2O)(ClO_4)](ClO_4)_3 \cdot 3H_2O \cdot 2CH_3OH$ ($C_{38}H_{52}Cl_4Fe_2N_8O_{23}$): C, 36.74; H, 4.22; N, 9.02. Found: C, 36.37; H, 4.26; N, 8.97.

$[Fe_2O(TPA)_2(OH)(H_2O)](ClO_4)_3$ (2a) was prepared by mixing TPA · $3HClO_4$ (0.591 g, 1.0 mmol) and Et_3N (0.455 g, 4.5 mmol) in 15 mL of methanol and $Fe(ClO_4)_3 \cdot 10H_2O$ (0.534 g, 1.0 mmol) in 5 mL of methanol. A dark green solid precipitated from the solution overnight in the refrigerator. ^{1}H NMR (CD_3CN, −40 °C): δ (ppm) 35.3, 27.2, and 21.4 (br, α-pyr or CH_2), 20.1, 18.9, 15.1, 14.2, and 13.0 (β-pyr), 8.4, 7.9, and 7.0 (γ-pyr). Anal. Calcd for $[Fe_2O(TPA)_2(OH)(H_2O)](ClO_4)_3 \cdot 2H_2O$ ($C_{36}H_{43}Cl_3Fe_2N_8O_{17}$): C, 40.12; H, 4.02; N, 10.40. Found: C, 40.22; H, 3.85; N, 10.22.

$[Fe_2O(5\text{-}Me\text{-}TPA)_2(OH)(H_2O)](ClO_4)_3$ (2b) was prepared by mixing 5-Me-TPA (0.166 g, 0.5 mmol) and Et_3N (0.101 g, 1.0 mmol) in 10 mL of methanol and $Fe(ClO_4)_3 \cdot 10H_2O$ (0.267 g, 0.5 mmol) in 5 mL of methanol. The reaction mixture was allowed to stand overnight at room temperature and then 10 mL of H_2O was added. Dark green microcrystals were obtained overnight in the refrigerator. ^{1}H NMR (CD_3CN, −40 °C): δ (ppm) 36.3, 27.7, and 20.7 (br, α-pyr or CH_2), 19.1, 17.1, 14.4, and 12.9 (β-pyr), 8.1, 7.6, 6.8, and 6.6 (γ-pyr), 4.0, 3.8, and 3.1 (5-CH_3). Anal. Calcd for $[Fe_2O(5\text{-}Me\text{-}TPA)_2(OH)(H_2O)](ClO_4)_3 \cdot 2H_2O$ ($C_{42}H_{55}Cl_3Fe_2N_8O_{17}$): C, 43.41; H, 4.77; N, 9.64; Cl, 9.15; Fe, 9.61. Found: C, 43.47; H, 4.60; N, 9.42; Cl, 9.12; Fe, 9.81.

$[Fe_2O(5\text{-}Et\text{-}TPA)_2(OH)(H_2O)](ClO_4)_3$ (2c) was prepared by mixing 5-Et-TPA · $3HClO_4$ (0.254 g, 0.376 mmol) and Et_3N (0.190 g, 1.88 mmol) in 8 mL of methanol and $Fe(ClO_4)_3 \cdot 10H_2O$ (0.201 g, 0.376 mmol) in 4 mL of methanol. The reaction mixture was allowed to stand overnight at room temperature and then $NaClO_4$ (0.461 g, 3.76 mmol) in 8 mL of H_2O was added. Dark green crystals of crystallographic quality were obtained from the solution upon standing at 4 °C. ^{1}H NMR (CD_3CN, −40 °C), δ (ppm): 36.0, 27.3, and 20.2 (br, α-pyr or CH_2), 18.3, 16.3, 13.5, and 12.1 (β-pyr), 7.3, 6.8, 6.1, and 5.7 (γ-pyr), 3.9, 3.4, and 2.8 (5-CH_2CH_3), 2.4 and 1.2 (5-CH_2CH_3). Anal. Calcd for $[Fe_2O(5\text{-}Et\text{-}TPA)_2(OH)(H_2O)](ClO_4)_3 \cdot 2H_2O \cdot CH_3OH$ ($C_{49}H_{71}Cl_3Fe_2N_8O_{18}$): C, 46.04; H, 5.60; N, 8.77. Found: C, 46.57; H, 5.60; N, 8.78.

$[Fe_2(O)_2(5\text{-}Me\text{-}TPA)_2](ClO_4)_3$ (3b) was prepared by adding 30% H_2O_2 solution in water (88 μL) into **2b** (0.300 g, 0.258 mmol) in 16 mL of CH_3CN at −40 °C. A dark green solid was isolated upon overnight standing at −40 °C and further purified by CH_3CN washing at −40 °C. Anal. Calcd for $[Fe_2(O)_2(5\text{-}Me\text{-}TPA)_2](ClO_4)_3$ ($C_{42}H_{48}Cl_3Fe_2N_8O_{14}$): C, 45.57; H, 4.37; N, 10.12; Cl, 9.61; Fe, 10.09. Found: C, 45.89; H, 4.18; N, 9.52; Cl, 10.13; Fe, 10.01.

Crystallographic Studies. X-ray diffraction data were collected on a red crystal of **1** with dimensions 0.500 × 0.250 × 0.200 mm^3 and a dark green crystal of **2c** with dimensions 0.550 × 0.500 × 0.500 mm^3 by an Enraf-Nonius CAD-4 diffractometer with graphite monochromated Mo Kα (λ = 0.71069 Å) radiation in the University of Minnesota Crystallography Facility. Cell constants and orientation matrixes for data collection were obtained from a least-squares refinement using the setting angles of 42 carefully centered reflections (2θ = 20.0−36.0°) for **1** and 44 carefully centered reflections (2θ = 30.0−52.0°) for **2c**. The intensities of three representative reflections were measured every 60 min of X-ray exposure time throughout the data collection to ascertain crystal integrity; no decay in intensity was observed. All data were corrected for empirical absorption and Lorentz and polarization effects. Pertinent crystallographic data and experimental conditions are summarized in Table 1.

Table 1. The Crystallographic Experiments and Computations[a] for **1** and **2c**

	1	**2c**
formula	$C_{36}H_{36}Cl_4Fe_2N_8O_{18}$	$C_{49}H_{71}Cl_3Fe_2N_8O_{18}$
formula wt, amu	1122.23	1278.20
temp, K	172	172
cryst system	monoclinic	monoclinic
space group	$P2_1/n$ (No. 14)	$P2_1/c$ (No. 14)
a, Å	11.577(6)	10.780(4)
b, Å	25.595(6)	23.88(2)
c, Å	15.428(7)	23.025(9)
β, deg	98.97(6)	96.78(3)
V, Å^3	4516(6)	5887(10)
Z	4	4
ϱ(calc), g cm^{-3}	1.651	1.433
radiation	Mo Kα (λ = 0.7107 Å)	Mo Kα (λ = 0.7107 Å)
$\mu_{(Mo\ K\alpha)}$, cm^{-1}	9.60	7.01
scan type	ω	ω
$2\theta_{max}$, deg	52.0	52.0
no. of reflcns	9065	11741
no. of unique data with $I > 2\sigma(I)$	4713	5694
No. of variables	613	704
R^b	0.083	0.099
$R_w{}^b$	0.072	0.099

[a] The intensity data were processed as described in: *CAD 4 and SDP-PLUS User's Manual*; B.A. Frenz & Assoc.; College Station, TX, 1982. The net intensity $I = [K(NPI)](C - 2B)$, where K = 20.1166 (attenuator factor), NPI = ratio of fastest possible scan rate to scan rate for the measurement, C = total count, and B = total background count. The standard deviation in the net intensity is given by $[\sigma(I)]^2 = (k/NPI)^2[C + 4B + (pI)^2]$ where p is a factor used to downweight intense reflections. The observed structure factor amplitude F_o is given by $F_o = (I/Lp)^{1/2}$, where Lp = Lorentz and polarization factors. The $\sigma(I)$'s were converted to the estimated errors in the relative structure factors $\sigma(F_o)$ by $\sigma(F_o) = 1/2[\sigma(I)/I]F_o$. [b] $R = (\sum||F_o| - |F_c||)/(\sum F_o)$; $R_w = \{(\sum w|F_o - F_c|^2)/(\sum w(F_o)^2)\}^{1/2}$.

The structures were solved by direct methods.[22] All non-hydrogen atoms were refined anisotropically, and hydrogen atoms were placed in calculated positions (d_{C-H} = 0.95 Å) and assigned thermal parameters that were 20% greater than the B_{equiv} value of the atom to which they were bonded and not refined. Refinement was carried out with full-matrix least squares on F with scattering factors from reference[23] and included anomalous dispersion terms.[24]

The structure of the cation, $[Fe_2O(TPA)_2(H_2O)(ClO_4)]^{3+}$ (**1**), is shown in Figure 1, together with the numbering scheme to the complex. The structure of the cation, $[Fe_2O(5\text{-}Et\text{-}TPA)_2(OH)(H_2O)]^{3+}$ (**2c**), is shown in Figure 2, together with the numbering scheme to the complex. The final fractional coordinates for **1** and **2c** are provided in the supplementary material, while selected bond lengths and angles for the complex cations are reported in Table 2. Complete listings of bond lengths and angles and thermal parameters are also included in the supplementary material.

(22) Gilmore, C. J. *J. Appl. Crystallogr.* **1984**, *17*, 42−46.
(23) Cromer, D. T.; Waber, J. T. In *International Tables for X-ray Crystallography*; Kynoch Press: Birmingham, England, 1974; Vol. IV, Table 2.2 A.
(24) Cromer, D. T.; Waber, J. T. In *International Tables for X-ray Crystallography*; Kynoch Press: Birmingham, England, 1974; Vol. IV, Table 2.3.1.

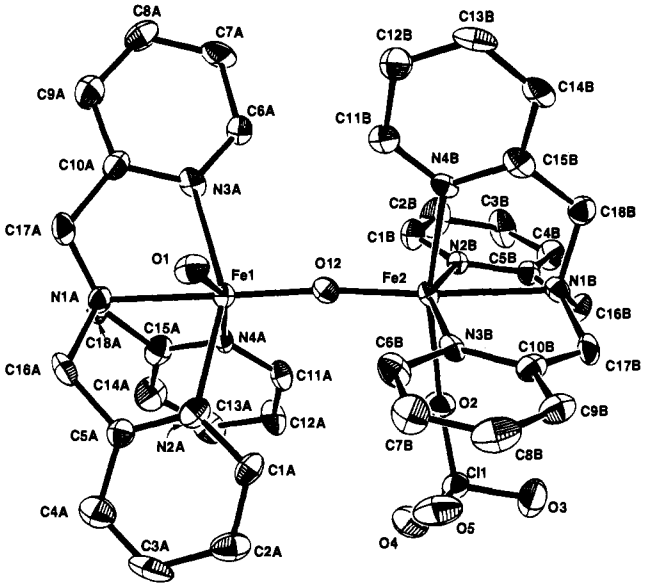

Figure 1. ORTEP plot of the cation of **1**, $[Fe_2O(TPA)_2(H_2O)(ClO_4)]^{3+}$, showing 50% probability ellipsoids. The hydrogen atoms are omitted for clarity.

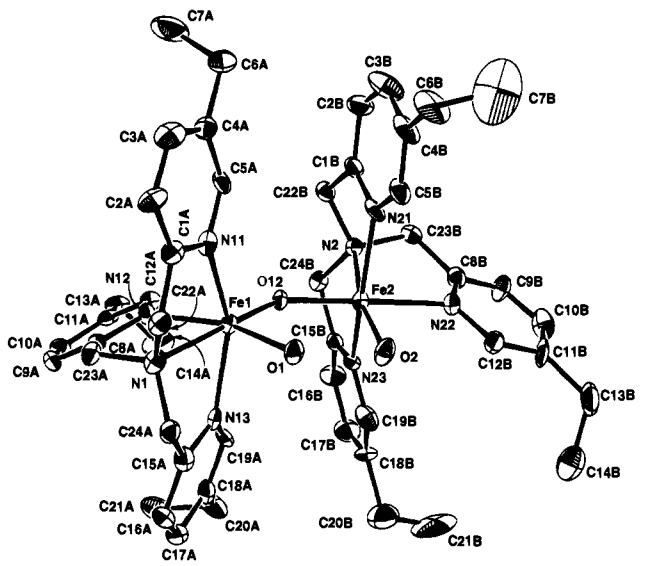

Figure 2. ORTEP plot of the cation of **2c**, $[Fe_2O(5\text{-}Et\text{-}TPA)_2(OH)(H_2O)]^{3+}$, showing 30% probability ellipsoids. The hydrogen atoms are omitted for clarity.

Physical Methods. Electrospray ionization mass spectral data were collected using a Sciex API III mass spectrometer (Sciex, Thornhill, Ontario, Canada). Cooled CH_3CN (dry ice on the syringe) was introduced by a syringe infusion pump (Model 22, Harvard Apparatus, South Natick, MA) through a 76 μm internal diameter fused silica capillary line at flow rates of 10 mL/min for about 20 min, and then the cooled sample solution (ca. 0.7 mM), which was prepared at −40 °C, was introduced. The instrument was scanned in 0.2-dalton steps and a 5 to 10 ms dwell time per step. Signal averaging was used to enhance the signal-to-noise ratio.

Low-temperature UV−vis spectra were recorded on a Hewlett Packard 8451 A diode array spectrophotometer by using an immersion dewar equipped with quartz windows. The low temperature was achieved by adding liquid nitrogen to the ethanol bath. Resonance Raman spectra were collected on a Spex 1403 spectrometer interfaced with a DM3000 data collection system using Spectra-Physics Models 2030-15 argon ion and 375B CW dye (Rhodamine 6G) lasers. Low-temperature spectra of **3** in CH_3CN solution were obtained at 77 K using a backscattering geometry. Samples were frozen onto a gold-plated copper cold finger in thermal contact with a dewar containing liquid nitrogen.[25] Raman frequencies were referenced to the intense feature at 922 cm^{-1} (ν_4) from frozen CH_3CN. Room-temperature Raman spectra of solids **2a**, **2b**, and **2c** were obtained from spinning KBr pellets using a 90° scattering geometry and Na_2SO_4 ($\nu_1(SO_4^{2-})$ = 998 cm^{-1}) as an internal standard. Slits were set for a band-pass of 4 cm^{-1} for all spectra.

^1H NMR spectra were obtained on Varian VXR 300 and VXR 500 spectrometers. Temperature calibration for low-temperature ^1H NMR experiments was accomplished with methanol. Chemical shifts (in ppm) are referenced to the residual protic solvent peaks. EPR spectra were obtained at liquid helium temperatures on a Varian E-109 spectrometer equipped with an Oxford cryostat. The Mössbauer spectrometers were run in the constant acceleration mode. The isomer shift is quoted relative to the centroid of Fe metal.

Magnetic susceptibility data were recorded on a Quantum Design SQUID susceptometer. Calibration and operation procedures have been reported elsewhere.[26] For $[Fe_2O(5\text{-}Et\text{-}TPA)_2(OH)(H_2O)](ClO_4)_3$ (**2c**), the data were collected over a temperature range of 10−300 K at a magnetic field of 0.5 T and were corrected for diamagnetism using Pascal's constants. The least-squares fit of the experimental data using

Table 2. Selected Bond Distances (Å) and Bond Angles (deg) for **1**, **2a**, and **2c**

(a) Bond Distances

	1		**2c**		**2a**[a]	
Fe1−μ−O	(O12)	1.791(7)	(O12)	1.779(5)	(O1)	1.780(6)
Fe2−μ−O	(O12)	1.783(7)	(O12)	1.826(5)	(O1)	1.839(6)
Fe1−O	(O1)	2.094(7)	(O1)	2.049(6)	(O2)	2.040(9)
Fe2−O	(O2)	2.140(7)	(O2)	1.907(7)	(O3)	1.913(7)
Fe1−N_{amine}	(N1A)	2.216(8)	(N1)	2.256(7)	(N10)	2.264(8)
Fe1−N_{py}	(N2A)	2.153(9)	(N11)	2.131(9)	(N11)	2.137(9)
	(N3A)	2.134(8)	(N12)	2.160(7)	(N21)	2.132(8)
	(N4A)	2.124(8)	(N13)	2.17(1)	(N31)	2.144(8)
Fe2−N_{amine}	(N1B)	2.237(8)	(N2)	2.217(7)	(N40)	2.194(8)
Fe2−N_{py}	(N2B)	2.118(8)	(N21)	2.146(9)	(N41)	2.128(9)
	(N3B)	2.100(8)	(N22)	2.246(8)	(N51)	2.245(7)
	(N4B)	2.100(8)	(N23)	2.127(9)	(N61)	2.124(9)
Fe1−Fe2		3.570(9)		3.346(9)		3.389(2)
O−O (H_3O_2)				2.464(9)		2.419(10)

(b) Bond Angles

	1		**2c**	**2a**[a]
Fe1−(μ-O)−Fe2	174.1(4)		136.3(3)	138.9(4)
Fe1−O⋯O−Fe2			20.5(9)	24.0(5)
O1−Fe1−O12	99.2(3)	O1−Fe1−O12	98.3(2)	
O1−Fe1−N1A	87.3(3)	O1−Fe1−N1	85.4(3)	
O1−Fe1−N2A	83.9(3)	O1−Fe−N11	88.8(3)	
O1−Fe1−N3A	87.0(3)	O1−Fe1−N13	91.1(3)	
N1A−Fe1−N4A	78.4(3)	N1−Fe1−N12	78.4(3)	
N1A−Fe1−N2A	78.0(3)	N1−Fe1−N11	76.9(3)	
N1A−Fe1−N3A	75.4(3)	N1−Fe1−N13	74.9(3)	
N4A−Fe1−O12	95.6(3)	N12−Fe1−O12	97.6(3)	
N4A−Fe1−N3A	99.5(3)	N12−Fe1−N11	92.5(3)	
N4A−Fe1−N2A	82.7(3)	N12−Fe1−N13	79.8(3)	
O12−Fe1−N2A	105.0(3)	O12−Fe1−N11	106.9(3)	
O12−Fe1−N3A	102.4(3)	O12−Fe1−N13	101.1(3)	
O2−Fe2−O12	96.9(3)	O2−Fe2−O12	97.5(3)	
O2−Fe2−N2B	82.0(3)	O2−Fe2−N22	90.7(3)	
O2−Fe2−N4B	166.0(3)	O2−Fe2−N21	104.3(4)	
O2−Fe2−N3B	86.9(3)	O2−Fe2−N23	102.7(3)	
N2B−Fe2−N1B	77.3(3)	N22−Fe2−N2	77.0(3)	
N2B−Fe2−N4B	97.3(3)	N22−Fe2−N21	90.1(3)	
N2B−Fe2−N3B	152.8(3)	N22−Fe2−N23	78.4(3)	
N1B−Fe2−O12	175.3(3)	N2−Fe2−O12	94.9(3)	
N1B−Fe2−N4B	78.6(3)	N2−Fe2−N21	75.1(3)	
N1B−Fe2−N3B	77.5(3)	N2−Fe2−N23	76.1(3)	
O12−Fe2−N4B	96.8(3)	O12−Fe2−N21	94.0(3)	
O12−Fe2−N3B	103.5(3)	O12−Fe2−N23	93.5(3)	

[a] Reference 27.

(25) Czemuszewicz, R. C.; Johnson, M. K. *Appl. Spectrosc.* **1983**, *37*, 297−298.

(26) O'Connor, C. J. *Prog. Inorg. Chem.* **1979**, *29*, 204−283.

Scheme 1

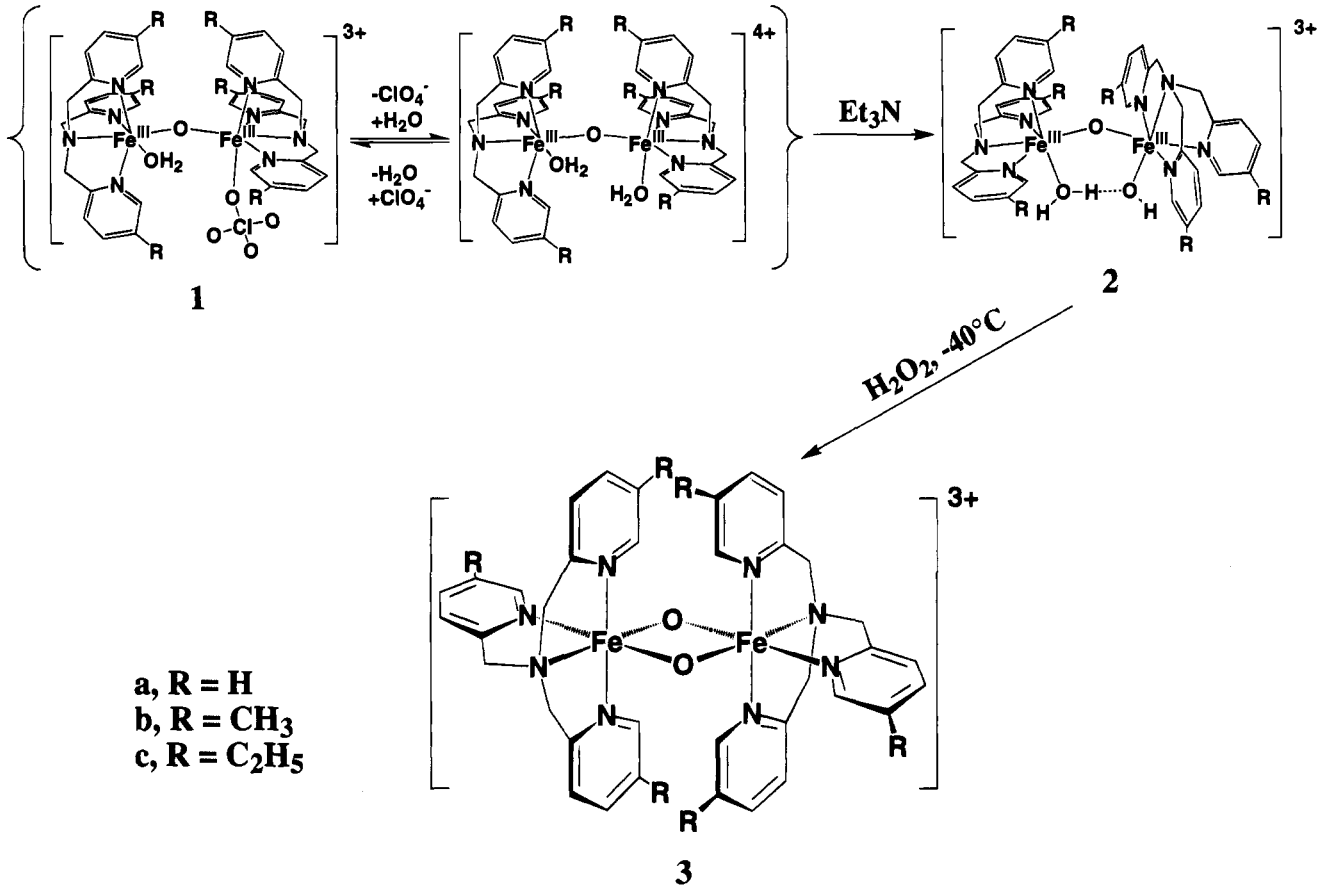

the Heisenberg–Dirac–van Vleck Hamiltonian ($\mathbf{H} = J\mathbf{S}_1 \cdot \mathbf{S}_2$) model with $S_1 = S_2 = {}^5/_2$ gave $J = 196$ cm^{-1}, $g = 2.0$, $p = 0.0083$, and TIP = 0 (where TIP is temperature-independent paramagnetism and p is fraction of a mononuclear $S = {}^5/_2$ impurity); these values are comparable to those reported for **2a**.[27]

For $[Fe_2(O)_2(5\text{-Me-TPA})_2](ClO_4)_3$ (**3b**), magnetic susceptibility data were collected over a temperature range of 4–220 K at four magnetic fields (0.1, 1.0, 3.0, and 5.0 T). A sample from the same batch was studied with Mössbauer spectroscopy; this study showed that 90% of the iron was present as **3b** with the remaining 10% in a (μ-oxo)diiron(III) form. Because the contaminating (μ-oxo)diiron(III) complex is strongly antiferromagnetically coupled, the contribution to the magnetization from the impurity is very small and was subtracted from the experimental data by assuming $J = 200$ cm^{-1}.[28]

X-ray absorption spectra (XAS) were collected at the Fe K-edge (~7.1 KeV) at the Stanford Synchrotron Radiation Laboratory (SSRL), the National Synchrotron Light Source (Brookhaven National Laboratory, Beam X-9A), and the Cornell High Energy Synchrotron Source (CHESS, station C-2). The monochromator was calibrated using the 7113.0 eV 1s → 3d peak in the XAS spectrum of $[Et_4N][FeCl_4]$. A_{exp}-(ln(C_o/C_t)) was determined from the counts observed from the incident (C_o) and the transmission (C_t) ionization detectors. After background correction and normalization, the energy value corresponding to a normalized edge absorption of 0.5 was designated the edge energy of a particular complex.

The treatment of the raw EXAFS data to yield χ is discussed at length in several review articles.[29,30] The refinements reported were on $k^3\chi$ data and the function minimized was $R = \{\sum k^6(\chi_c - \chi)^2/n\}^{1/2}$, where the sum is over n data points between 2.0 and 13 Å^{-1}. Single-scattering EXAFS theory allows the total EXAFS spectrum to be described as the sum of shells of separately modeled atoms as shown below.

$$\chi(k) = \sum_{\text{shells}} nA[f(k)k^{-1}r^{-2}\exp(-2\Delta\sigma^2k^2)\sin[2kr + \alpha(k)]]$$

where n is the number of atoms in a shell, $k = [8\pi^2m_e(E - E_0 + \Delta E)/h^2]^{1/2}$, and $\exp(-2\Delta\sigma^2k^2)$ is the Debye–Waller factor. The amplitude reduction factor (A) and the shell-specific edge shift (ΔE) are empirical parameters that partially compensate for imperfections in the theoretical amplitude and phase functions f and α.[31] The analysis procedure, a variation of FABM (fine adjustment based on models),[32] uses theoretical amplitude and phase functions calculated using a curved-wave formalism.[33] For each shell, crystallographically characterized model complexes such as $[Fe^{III}(acac)_3]$ are used to determine A and ΔE.[31] This leaves two parameters per shell (r and n or $\Delta\sigma^2$) to be refined instead of the four parameters refined using BFBT ("best fit based on theory").[32] In fitting the EXAFS data for complex **3b**, we did not make any attempt to remove the contribution of the (μ-oxo)diiron(III) contaminant that represents 10% of the sample.

Electrochemical studies were performed with a BAS 100 electrochemical analyzer (Bioanalytical Systems, Inc. West Lafayette, IN). All experiments were performed at −40 °C in acetonitrile with 0.1 M tetrabutylammonium tetrafluoroborate as the supporting electrolyte. Cyclic voltamograms (CV) were obtained by using a three-component system consisting of a platinum disk working electrode, a platinum wire auxiliary electrode, and a silver wire as the reference electrode. Potentials were corrected to the NHE standard by measuring the ferrocenium/ferrocene couple under the same conditions.

(27) Hazell, A.; Jensen, K. B.; McKenzie, C. J.; Toftlund, H. *Inorg. Chem.* **1994**, *33*, 3127–3134.
(28) Norman, R. E.; Yan, S.; Que, L., Jr.; Backes, G.; Ling, J.; Sanders-Loehr, J.; Zhang, J. H.; O'Connor, C. J. *J. Am. Chem. Soc.* **1990**, *112*, 1554–1562.
(29) Teo, B.-K. In *EXAFS Spectroscopy, Techniques and Applications*; Teo, B.-K., Joy, D. C., Eds.; Plenum: New York, 1981; pp 13–58.
(30) Scott, R. A. *Methods Enzymol.* **1985**, *11*, 414–459.
(31) Teo, B.-K. *J. Am. Chem. Soc.* **1979**, *101*, 2815–2832.
(32) Teo, B.-K.; Antonio, M. R.; Averill, B. A. *J. Am. Chem. Soc.* **1983**, *105*, 3751–3762.
(33) McKale, A. G.; Veal, B. W.; Paulikas, A. P.; Chan, S.-K.; Knapp, G. S. *J. Am. Chem. Soc.* **1988**, *110*, 3763–3768.

Results and Discussion

Structural and Spectroscopic Properties of the Precursor Complex. The precursor complex for the high-valent species is a (μ-oxo)diiron(III) TPA complex which is formed from the reaction of $Fe(ClO_4)_3$, TPA, and Et_3N. This reaction is quite sensitive to the amount of base added and two distinct complexes can be obtained, $[Fe_2O(L)_2(H_2O)(ClO_4)](ClO_4)_3$ (**1**) and $[Fe_2O(L)_2(OH)(H_2O)](ClO_4)_3$ (**2**). The two complexes are related to each other by acid–base chemistry; **1** converts to **2** by the addition of 1 equiv of base (Scheme 1). Both complexes have now been characterized by X-ray crystallography.[34]

$[Fe_2O(TPA)_2(H_2O)(ClO_4)](ClO_4)_3$, **1**, is a nearly linear (μ-oxo)diiron(III) complex (Figure 1) with an Fe–O–Fe angle of 174.1(4)° and an Fe–Fe distance of 3.570(9) Å (Table 2). Complex **1** has Fe–μ-O bond lengths of 1.791(7) (Fe1–O12) and 1.783(7) Å (Fe2–O12), which are typical of such bonds.[35] The TPA ligands are coordinated with the tertiary amines trans to the oxo bridge, so all six Fe–N_{py} bonds are comparable in length (2.100–2.153 Å, average 2.122 Å). The absence of a strongly coordinating oxyanion results in shorter Fe–N_{py} bonds than those found in corresponding (μ-oxo)diiron(III) TPA complexes with bridging anions (average Fe–N_{py} bonds of 2.2 Å).[28,36] Terminally coordinated aqua (Fe1–O1 = 2.094(7) Å) and perchlorato (Fe2–O2 = 2.140(7) Å) ligands complete the respective iron coordination spheres. The structure of **1** is similar to that of $[Fe_2O(tmima)_2(H_2O)_2](ClO_4)_4$, which also has terminal aqua ligands.[37]

Complex **2** is effectively the conjugate base of **1**; we have solved the structure of **2c** where L = 5-Et-TPA (Figure 2). Complex **2c** has a bent (μ-oxo)diiron(III) unit supported by a bridging $H_3O_2^-$ anion and a structure which is comparable to that recently reported for **2a** (L = TPA).[27] Both iron atoms have distorted octahedral geometries with the nitrogen atoms of the 5-Et-TPA ligands completing the coordination spheres. The presence of the $H_3O_2^-$ bridge is indicated by a short O1–O2 separation (2.464(9) Å) (Table 2), indicative of a strong hydrogen bond that characterizes such bridges in other metal complexes.[27,38] The torsional angle of Fe1-O1–O2-Fe2 is 20.5°. The Fe1–O1 bond length is 2.049(6) Å which is comparable in length to those of other terminal Fe^{III}–OH_2 distances.[39] The Fe2–O2 bond length (1.907(7) Å) is much shorter, allowing us to assign O2 as the hydroxide component of the $H_3O_2^-$ bridge. Notably, complexes **2** are the only ones in which all three ionization states of water are represented.

The presence of the $H_3O_2^-$ bridge has important consequences for the geometry of the (μ-oxo)diiron(III) unit. The (μ-oxo)diiron(III) unit has Fe–μ-O bonds of 1.779(5) (Fe1–O12) and 1.826(5) Å (Fe2–O12), which are in the range found for oxo bridges.[35] The unsymmetric Fe–O–Fe core can be ascribed to the differing Lewis acidities of the iron centers as a result of having an aqua ligand on Fe1 and a hydroxo ligand on Fe2. The $H_3O_2^-$ bridge also engenders an Fe–O–Fe angle of 136.3-

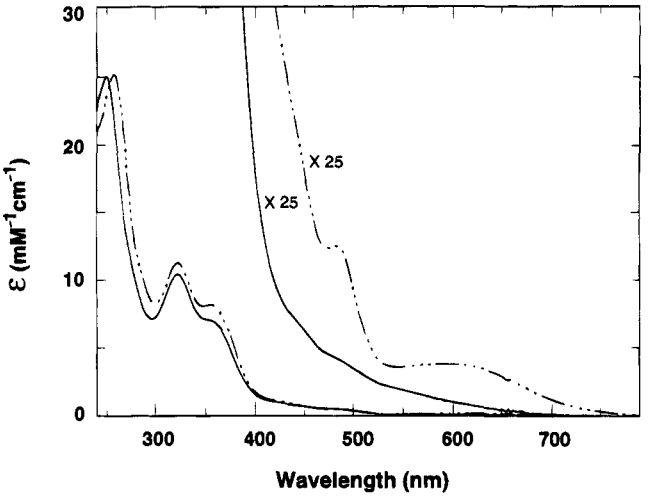

Figure 3. UV–vis spectra of **1** (—) and **2b** (— ··· —) in CH_3CN at −40 °C.

(3)° and a Fe–Fe distance of 3.346(9) Å, making it comparable in bite to the phosphato bridge in $[Fe_2O(TPA)_2\{O_2P(OPh)_2\}](ClO_4)_3$.[28] The bending of the Fe–O–Fe unit forces the 5-Et-TPA ligands to adopt different coordination orientations relative to the oxo bridge in order to avoid interligand steric interactions; this has been noted for a number of (μ-oxo)diiron(III) TPA complexes with Fe–O–Fe angles less than 143°.[28,36] Thus, the tertiary amine nitrogen on Fe1 is coordinated *trans* to the oxo bridge, while that on Fe2 is bound *cis* to the oxo bridge and *trans* to the terminal hydroxide. As a result, the Fe–N_{py} bond *trans* to the oxo bridge (Fe2–N22, 2.246(8) Å) is significally longer than the other five (2.127–2.170 Å, average 2.147 Å); such a difference (~0.1 Å) between *cis* and *trans* Fe–N_{py} distances is comparable to that found in $[Fe_2O(TPA)_2(MoO_4)](ClO_4)_2$.[36]

Though the structure of **2c** is similar to that recently reported for **2a**,[27] the presence of the 5-ethyl groups engenders a few differences (Table 2). Complex **2c** has a shorter Fe–Fe separation than **2a** presumably due to the slightly shorter Fe2–μ-O bond and smaller Fe–O–Fe angle in **2c**. The average Fe–N_{py} bond in **2c** in turn is slightly longer than that found in **2a**. These structural differences are also reflected in the spectroscopic properties of the complexes (*vide infra*).

Complexes **1** and **2** have distinct physical properties that derive from their structures. Complex **1** is red in color as a result of the tailing of intense oxo-to-iron(III) charge transfer bands in the UV region into the visible region (Figure 3) as expected for a nearly linear Fe–O–Fe unit.[36b] Furthermore, **1** exhibits paramagnetically shifted ^1H NMR features in the region expected for (μ-oxo)diiron(III) TPA complexes (Figure 4); the small number of peaks observed indicates that the TPA ligand has essentially 3-fold symmetry in solution, suggesting that the terminal aqua and perchlorato ligands are labile in solution. The Mössbauer spectra of **1** consist of one quadrupole doublet with properties (Table 3) typical of an antiferromagnetically coupled (μ-oxo)diiron(III) complex.[35]

Complex **2** has a green color resulting from the presence of a bent Fe–O–Fe unit.[36] Characteristic bands are observed at ~360, ~485, and ~605 nm (Figure 3), similar to those observed for phosphate- and molybdate-bridged (μ-oxo)diiron(III) TPA complexes. Based on our earlier correlations,[28,36] these features suggest an Fe–O–Fe angle of approximately 140°, in agreement with the crystal structure. Complex **2** has an NMR spectrum more complicated than that of **1** but typical of a (μ-oxo)diiron(III) TPA complex with distinct iron sites (Figure 4).[28,36] Thus, **2** appears to maintain its structure in solution.

(34) These structures were briefly communicated in: Wilkinson, E. C.; Dong, Y.; Que, L., Jr. *J. Am. Chem. Soc.* **1994**, *116*, 8394–8395.

(35) Kurtz, D. M., Jr. *Chem. Rev.* **1990**, *90*, 585–606.

(36) (a) Holz, R. C.; Elgren, T. E.; Pearce, L. L.; Zhang, J. H.; O'Connor, C. J.; Que, L., Jr. *Inorg. Chem.* **1993**, *32*, 5844–5850. (b) Norman, R. E.; Holz, R. C.; Menage, S.; O'Connor, C. J.; Zhang, J.; Que, L., Jr. *Inorg. Chem.* **1990**, *29*, 4629–4637.

(37) Buchanan, R. M.; Chen, S.; Richardson, J. F.; Bressan, M.; Foti, L.; Morvillo, A.; Fish, R. H. *Inorg. Chem.* **1994**, *33*, 3208–3209.

(38) Ardon, M.; Bino, A. *Struct. Bonding (Berlin)* **1987**, *65*, 1–27.

(39) (a) Murch, B. P.; Bradley, F. C.; Boyle, P. D.; Papeafthymiou, V.; Que, L., Jr. *J. Am. Chem. Soc.* **1987**, *109*, 7993–8003. (b) Ou, C.-C.; Lalancette, R. A.; Potenza, J. A.; Schugar, H. J. *J. Am. Chem. Soc.* **1978**, *100*, 2053–2057. (c) Thich, J. A.; Ou, C.-C.; Powers, D.; Vasilious, B.; Mastropaolo, D.; Potenza, J. A.; Schugar, H. J. *J. Am. Chem. Soc.* **1976**, *98*, 1425–1432.

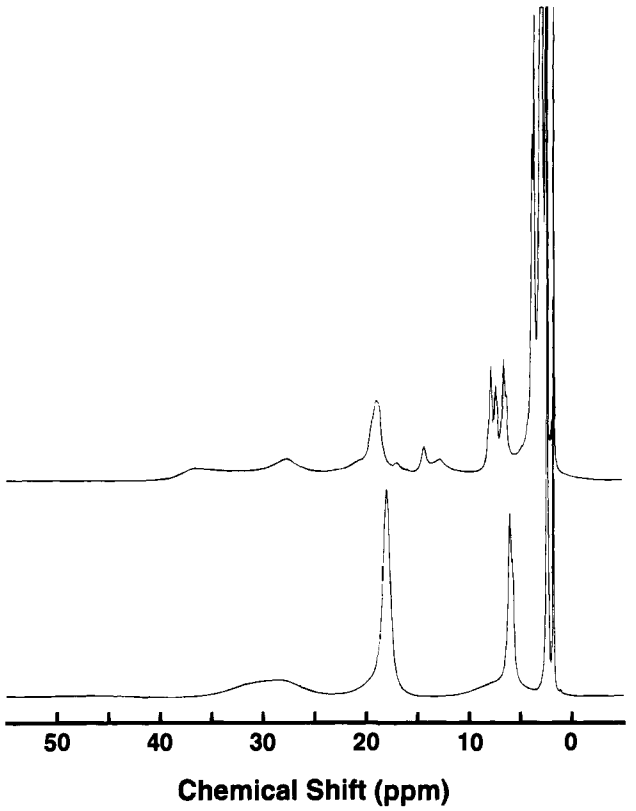

Figure 4. ^{1}H NMR spectra of **1** (bottom) and **2b** (top) in CD_3CN at −40 °C.

Table 3. Hyperfine Parameters of Diiron Complexes at 4.2 K

compd	δ^a (mm/s)	ΔE_Q(**1**) (mm/s)	η(**1**)	ΔE_Q(**2**) (mm/s)	η(**2**)
1 (solid)[c]	0.45(2)	−1.67(3)	0.4(3)	−1.67(3)	0.5(3)
2b (solid)[c]	0.45(2)	−1.59(3)	0.3(3)	−0.94(3)	~1.0
2b (soln)[c]	0.45(2)	−1.63(3)	0.2(3)	−1.11[b]	0.7(3)
2c (solid)[c]	0.45(2)	−1.70(3)	0.4(3)	−0.99(3)	~1.0
3b (solid)[d]	0.14(2)	+0.49(3)	0.3(3)	+0.49(3)	0.3(3)
3b + ferrocene[c]	0.45(2)	1.51(3)		1.27(3)	

[a] Within the resolution of the Mössbauer data, the isomer shifts (quoted at 4.2 K relative to iron metal at 298 K) of site 1 and site 2 are the same for all complexes. [b] The value reported here represents the average of a distribution of ΔE_Q for site 2. [c] $S = 0$. [d] $S = {}^3/_2$.

Further spectroscopic studies of **2** provide additional insight. Raman spectra of **2a**, **2b**, and **2c** show resonance-enhanced vibrations at 450, 458, and 462 cm^{-1}, respectively. When **2b** is prepared in the presence of $^{18}OH_2$, the vibration at 458 cm^{-1} shifts to 446 cm^{-1}. We thus assign it to the symmetric Fe−O−Fe stretch that is typically seen for (μ-oxo)diiron(III) complexes.[40] The energy of this vibration is dependent on the Fe−O−Fe angle and shifts to lower energy as the angle increases. Based on the secular equations derived by Wing and Callahan[41] and the observed ^{18}O shift, the Fe−O−Fe angle of **2b** is calculated to be 138°, in good agreement with the crystallographically observed angle for **2c** (136.3(3)°) and the correlations of Sanders-Loehr *et al.*[40] Furthermore, the smaller ν_s(Fe−O−Fe) observed for **2a** is entirely consistent with its crystallographically observed larger Fe−O−Fe angle of 138.9(4)°.[27]

The 4.2 K Mössbauer spectrum of *polycrystalline* **2b** (Figure 5B) exhibits a nested pair of symmetric doublets with quadrupole splittings and isomer shifts typical of high-spin Fe^{III} sites.[35]

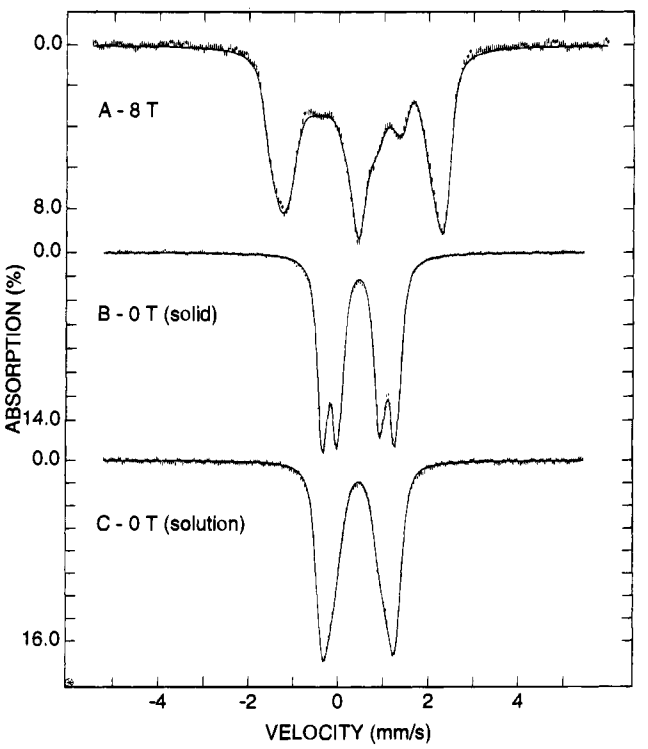

Figure 5. Mössbauer spectra of **2b** in frozen acetonitrile solution (A and C) and as a polycrystalline solid (B). The solid lines in A and B are least-squres fits to the spectra. The solid line drawn through the 8.0 T spectrum is a spectral simulation using the parameters listed in Table 3.

Figure 5C shows a zero-field spectrum of a sample containing **2b** dissolved in acetonitrile. Spectral decomposition of the spectrum into two quadrupole doublets shows that the parameters of site 1 are essentially the same as observed in the solid. The parameters of site 2, however, differ in the polycrystalline state and in solution. The ΔE_Q of site 2 is 18% larger in the solution sample. Moreover, the line width of doublet 2 has increased from 0.27 mm/s in the solid to 0.40 mm/s (Voigt shape) in solution, suggesting that ΔE_Q of site 2 is distributed about a mean value $\Delta E_Q(2) = 1.11$ mm/s. Thus, the ligand environment of site 2 exhibits some structural disorder in frozen acetonitrile solution. Comparison of the structures of **1** and **2** suggests that the smaller ΔE_Q value of **2** corresponds to Fe2, the iron center with the hydroxo ligand. Figure 5A shows the CH_3CN spectrum recorded at 4.2 K in an applied magnetic field of 8.0 T; the solid line drawn through the data is a theoretical spectrum computed with the assumption that both Fe^{III} sites reside in a diamagnetic environment. The parameters listed in Table 3, together with the observed diamagnetism, confirm that **2b** contains an antiferromagnetically coupled $Fe^{III}Fe^{III}$ pair.

Generation of the High-Valent Species and Its Isolation. The addition of H_2O_2 to **2** (L = TPA, 5-Me-TPA, or 5-Et-TPA) in CH_3CN at −40 °C generates a transient bright green species **3** exhibiting an intense visible absorption band with a maximum at 614−616 nm (Figure 6) and a rhombic $S = {}^3/_2$ EPR spectrum with $g = 4.45$, 3.90, and 2.01 (Figure 7). Similar treatment of **1** does not elicit this green intermediate.[42] Species **3** persists for 1−2 h at −40 °C in the case of L = TPA and longer for 5-alkyl-TPA complexes.

In the case of 5-Me-TPA, a green solid **3b** can be isolated upon overnight standing at −40 °C, which is further purified by repeated washing with CH_3CN at −40 °C. As observed

(40) Sanders-Loehr, J.; Wheeler, W. D.; Shiemke, A. K.; Averill, B. A.; Loehr, T. M. *J. Am. Chem. Soc.* **1989**, *111*, 8084−8093.
(41) Wing, R. M.; Callahan, K. P. *Inorg. Chem.* **1969**, *8*, 871−874.
(42) Instead **1** reacts with H_2O_2 to afford a purple intermediate whose characterization is in progress.

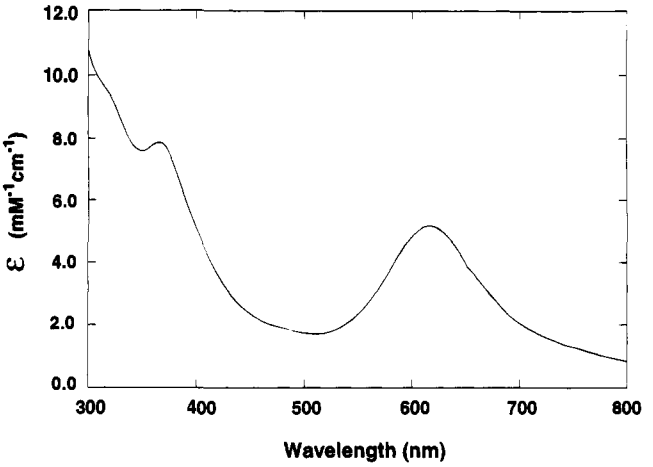

Figure 6. UV−vis spectrum of **3b** in CH_3CN at −40 °C. The molar extinction coefficients are based on the concentration of **3b** derived from EPR integration.

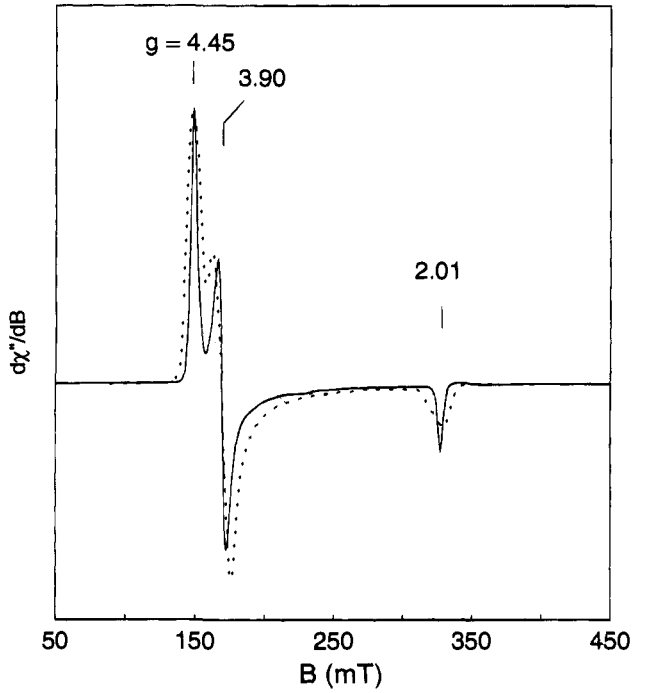

Figure 7. EPR spectra of **3b** in CH_3CN (3.9 mM, —) and as a powder (9.9 mg, - - -). Experimental conditions: temperature, 20 K; microwaves, 0.2 mW at 9.23 GHz; modulation, 1 mT at 100 kHz; gain, 500 (CH_3CN).

previously for the 100 K Mössbauer spectrum of **3a** generated *in situ*, complex **3b** displays one sharp (Γ = 0.27 mm/s) quadrupole doublet; for **3b** we observe $\delta = 0.12 \pm 0.01$ mm/s and $\Delta E_Q = 0.49$ mm/s. This doublet accounts for about 90% of the iron in the Mössbauer sample (Figure 8). The remaining 10% has parameters typical of a (μ-oxo)diiron(III) species with spectral properties quite similar, if not identical, to those of the starting material of Figure 5B; its contribution is indicated by the solid line drawn above the data of Figure 8A. We thus have a preparation of **3b** of fairly high purity.

Elemental analysis of **3b** yielded the following values: C, 45.89; H, 4.18; N, 9.52; Cl, 10.13; Fe, 10.01. The respective ratios of C/Fe and N/Fe of 21 and 3.8 indicate the presence of one 5-Me-TPA ligand per Fe, while the Cl/Fe ratio of 1.6 minimally requires a complex with 2 Fe and 3 ClO_4. Electrospray ionization mass spectral studies on **3b** corroborate the ratios derived from elemental analysis and show that there is a cluster of positive ions with $m/z \geq 1006$, corresponding to

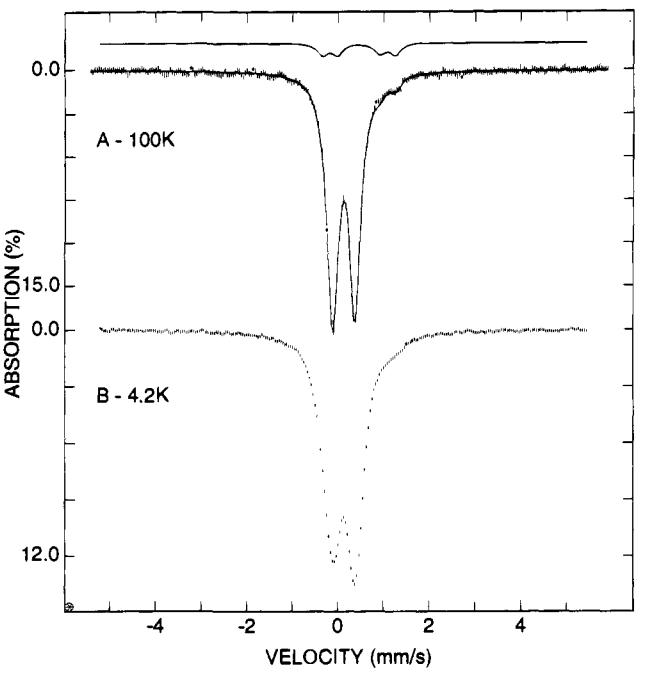

Figure 8. Mössbauer spectra of solid **3b** recorded in zero field at the temperatures indicated. The solid line in (A) is a least-squares fit to one quadrupole doublet for the majority species **3b** (91%) and two doublets for the minority $Fe^{III}Fe^{III}$ species; the contribution of the latter is shown separately above the data. At 100 K, complex **3b** has ΔE_Q = 0.49 mm/s and δ = 0.12 mm/s.

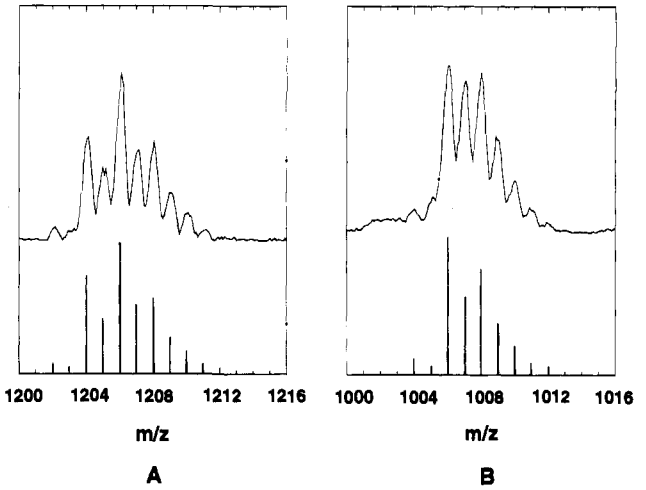

Figure 9. Negative (A) and positve ion (B) electrospray ionization mass spectra of **3b** obtained on a Sciex API III mass spectrometer. The upper traces show the experimental data, while the bars below represent the isotopic distributions calculated for $\{[Fe_2(O)_2(5\text{-Me-TPA})_2](ClO_4)_4\}^-$ (A) and $\{[Fe_2(O)_2(5\text{-Me-TPA})_2](ClO_4)_2\}^+$ (B).

$\{[Fe_2(O)_2(5\text{-Me-TPA})_2](ClO_4)_2\}^+$, and a cluster of negative ions with $m/z \geq 1204$, corresponding to the ion $\{[Fe_2(O)_2(5\text{-Me-TPA})_2](ClO_4)_4\}^-$ (Figure 9). Both ions exhibit isotope intensity patterns that closely match the calculated patterns. Furthermore, in view of our earlier results,[17] we have searched the positive ion mass spectrum for the presence of $\{[FeO(5\text{-Me-TPA})](ClO_4)_2\}^+$ and found no evidence for such an ion. Therefore, **3b** is best formulated as the dinuclear complex $[Fe_2(O)_2(5\text{-Me-TPA})_2](ClO_4)_3$.

Evidence for an $Fe_2(\mu\text{-}O)_2$ Core. The EXAFS data for **3b** provide a strong indication of the nature of the diiron core. The r'-space spectrum of **3b** exhibits prominent and comparably intense features centered at r' = 1.3 and 2.4 Å (Figure 10A), where the metal-scatterer distance r approximately equals r' +

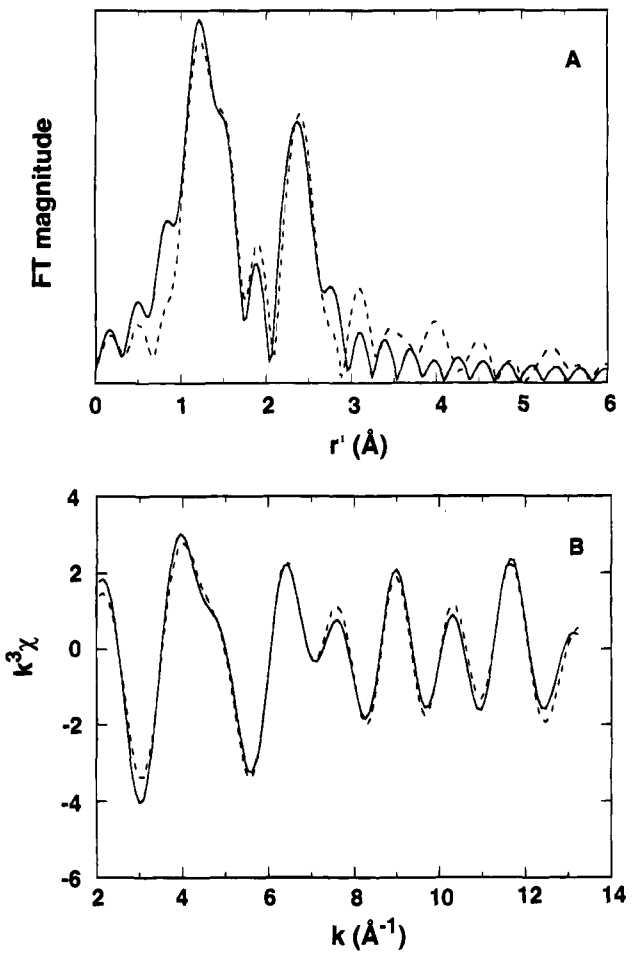

Figure 10. EXAFS data (k = 2−13 Å^{-1}) (- - -) and simulations (—) for **3b**: (A) r'-space spectrum; (B) k-space spectrum.

0.4 Å.[30] The large intensity of the second-sphere feature is unusual and suggests the presence of a scatterer or scatterers at ca. 2.7−3.0 Å with little vibrational disorder. Such a prominent feature is not observed in $[Fe_2O(\mu\text{-}XO_2)_nL_2]$ complexes (XO_2 = carboxylate, phosphate, molybdate; n = 0, 1, 2)[8b] but is found for $[Fe^{III}_2(\mu\text{-}O)(\mu\text{-}OH)(6\text{-Me-TPA})_2](ClO_4)_3$[43] (**4**) and corresponds to its crystallographically determined 2.94(1) Å Fe−Fe distance. Similarly, the r' = 2.4 Å feature observed for **3b** can only be fit with an Fe scatterer at 2.89 Å (Table 4); this is a distance shorter than those found for $Fe^{III}_2(\mu\text{-}OR)_2$[39c,44] complexes but comparable to that found for **4**. Given the mass established for **3b**, the most reasonable structure that can accommodate the Fe−Fe distance is an $Fe_2(\mu\text{-}O)_2$ rhomb akin to those of $Mn_2(\mu\text{-}O)_2$ complexes,[45] making **3** the first bis(μ-oxo)diiron complex thus far observed (Scheme 1).[46]

Fits to the k-space EXAFS spectrum (Figure 10B) are summarized in Table 4. A minimum of three shells is required to simulate the first coordination sphere features well (fits 1−7). The best fit that encompasses both first and second coordination spheres (fit 13) consists of 1 N/O at 1.77 Å, 3 N/O at 1.94 Å, 2 N/O at 2.17 Å, and 1 Fe at 2.89 Å. The negative $\Delta\sigma^2$ value associated with the 1.77 Å scatterer reflects the smaller degree of vibrational disorder associated with a short Fe−O bond relative to that associated with the 1.99 Å Fe−O bonds of Fe(acac)$_3$[47] used as the standard for oxygen scatterers in our protocol; such negative $\Delta\sigma^2$ values have been found for the oxo bridges of (μ-oxo)diiron(III) complexes.[43,48] Doubling the number of scatterers in the 1.77 Å shell (fit 11) increases the distance to 1.83 Å, which is essentially the average of the 1.77 Å scatterer and a ca. 1.89 Å scatterer derived from the 1.94 Å shell of fit 13. This fit was discarded because of the negative $\Delta\sigma^2$ values obtained for the ~2 Å shell, which is unreasonable. Based on fit 13, the Fe−O bonds to the Fe_2O_2 core would then correspond to the scatterer at 1.77 Å and one of the scatterers in the 1.94-Å shell, while the Fe−N bonds of the 5−Me−TPA ligand would be associated with the remaining scatterers in the fit.

The Fe_2O_2 rhomb proposed for **3b** would thus have sides of different lengths. Such distortions in the M_2O_2 rhomb are not unusual. The Fe−O bond lengths in $[Fe^{III}_2(\mu\text{-}O)_2(6\text{-Me-TPA})_2](ClO_4)_2$ are 1.841(4) and 1.917(4) Å, respectively, which differ by 0.08 Å,[46] while those in complexes with $Fe^{III}_2(\mu\text{-}OR)_2$ (R = H or alkyl) cores typically differ by 0.05−0.07 Å.[39b,44a] The EXAFS analysis for **3b** does not allow us to distinguish whether the Fe−μ-O bond lengths differ because of a charge-localized structure as in $[Mn_2O_2(TPA)_2]^{3+}$ [45b] or unsymmetrically bridged oxo groups as in the $Fe^{III}_2(\mu\text{-}O)_2$ and $Fe^{III}_2(\mu\text{-}OR)_2$ complexes,[39b,44a,46] but the Mössbauer data of **3b** show equivalent iron sites even at 1.5 K, strongly disfavoring the charge-localized model.

The resonance Raman spectra of **3a** and **3b** support the proposed $Fe_2(\mu\text{-}O)_2$ structure. The TPA intermediate exhibits an enhanced (λ_{ex} = 614 nm) vibration at 666 cm^{-1}, while the corresponding 5-Me-TPA species shows a Fermi doublet at 676 and 656 cm^{-1} (Figure 11). These features shift to 638 (for **3a**) and 634 (for **3b**) cm^{-1}, upon addition of $H_2{}^{18}O$ but are unaffected by the presence of D_2O. The facile exchange with water excludes the possibility that this vibration arises from an O−O stretch, since the exchange would entail breaking and re-forming the O−O bond. The observed isotope shifts are consistent with that predicted for a diatomic Fe−O vibration ($\Delta\nu_{calcd}$ = 29 cm^{-1}), but 666 cm^{-1} is low for an Fe=O bond (*e.g.* ~850 cm^{-1} for [(TPP)FeO] and [(salen)FeO][49]) and high for an Fe−OH bond (*e.g.* 541 cm^{-1} for $[Fe(T(2\text{-N-Me})PyP)OH]^{4+}$ [50]). On the other hand, a strongly enhanced and ^{18}O-sensitive feature is observed near 700 cm^{-1} for $Mn_2O_2{}^{3+}$ complexes; this vibration has been assigned to a breathing mode of the Mn_2O_2 core.[51] It would thus be reasonable to associate the 666-cm^{-1} band of **3** with an analogous mode of the Fe_2O_2 core.

The 400-cm^{-1} regions of the Raman spectra of **3a** and **3b** are rich in features; these are likely to be metal−ligand vibrations as evidenced by the shifts observed when TPA is substituted with 5-Me-TPA. One of these vibrations in each complex is sensitive to the addition of $H_2{}^{18}O$ (Figure 11C), suggesting the coupling of an Fe_2O_2 mode to one of the Fe−N

(43) Zang, Y.; Pan, G.; Que, L., Jr.; Fox, B. G.; Münck, E. *J. Am. Chem. Soc.* **1994**, *116*, 3653−3654.
(44) (a) Borer, L.; Thalken, L.; Ceccarelli, C.; Glick, M.; Zhang, J. H.; Reiff, W. M. *Inorg. Chem.* **1983**, *22*, 1719−1724. (b) Chiari, B.; Piovesana, O.; Tarantelli, T.; Zanazzi, P. F. *Inorg. Chem.* **1984**, *23*, 3398−3404. (c) Snyder, B. S.; Patterson, G. S.; Abrahamson, A. J.; Holm, R. H. *J. Am. Chem. Soc.* **1989**, *111*, 5214−5223.
(45) (a) Wieghardt, K. *Angew. Chem., Int. Ed. Engl.* **1989**, *28*, 1153−1172. (b) Towle, D. K.; Botsford, C. A.; Hodgson, D. J. *Inorg. Chim. Acta* **1988**, *141*, 167−168.
(46) We very recently communicated the first crystal structure of a bis(μ-oxo)diiron(III) complex, $[Fe_2(\mu\text{-}O)_2(6\text{-Me-TPA})_2](ClO_4)_2$. Zang, Y.; Dong, Y.; Que, L., Jr.; Kauffmann, K.; Münck, E. *J. Am. Chem. Soc.* **1995**, *117*, 1169−1170.
(47) Iball, J.; Morgan, C. H. *Acta Crystallogr.* **1967**, *23*, 239−244.
(48) Scarrow, R. C.; Maroney, M. J.; Palmer, S. M.; Roe, A. L.; Que, L., Jr.; Salowe, S. P.; Stubbe, J. *J. Am. Chem. Soc.* **1987**, *109*, 7857−7864.
(49) Proniewicz, L. M.; Bajdor, K.; Nakamoto, K. *J. Phys. Chem.* **1986**, *90*, 1760−1766.
(50) Reed, R. A.; Rodgers, K. R.; Kushmeider, K.; Spiro, T. G.; Su, Y. O. *Inorg. Chem.* **1990**, *29*, 2881−2883.
(51) (a) Czemuszewicz, R. S.; Dave, B.; Rankin, J. G. In *Spectroscopy of Biological Molecules*; Hester, R. E., Girling, R. B., Eds.; Royal Society of Chemistry: Cambridge, 1991; pp 285−288. (b) Gamelin, D. R.; Kirk, M. L.; Stemmler, T. L.; Pal, S.; Armstrong, W. H.; Penner-Hahn, J. E.; Solomon, E. I. *J. Am. Chem. Soc.* **1994**, *116*, 2392−2399.

Table 4. One- to Four-Shell Restricted Fits to the Fourier-Filtered First-Sphere $k^3\chi$ Data of **3b**[a]

	Fe−O/N						Fe−Fe						
fit no.	n	r	$\Delta\sigma^2$	n	r	$\Delta\sigma^2$	n	r	$\Delta\sigma^2$	n	r	$\Delta\sigma^2$	R (%)
1[b]	6	1.938	0.0241										29.2
2[b]	2	1.823	0.0125				4	2.031	0.0159				30.8
3[b]	2	1.827	−0.0002	3	2.042	−0.0008	1	2.251	−0.0050				10.9
4[b]	2	1.828	0.0029	2	2.008	0.0009	2	2.164	0.008				7.0
5[b]	1	1.796	−0.0001	2	1.966	0.00287	3	2.091	−0.0177				7.7
6[b]	1	1.795	−0.0036	4	2.0055	0.00373	1	2.252	−0.0031				6.4
7[b]	1	1.787	−0.0045	3	1.962	0.0012	2	2.211	0.0036				11.5
8[c]	2	1.836	0.0015	2	2.019	−0.0007	2	2.187	0.006				51.8
9[c]	1	1.821	−0.0011	4	2.008	0.0086	1	2.264	−0.0014				51.6
10[c]	1	1.801	−0.0012	3	1.979	0.0032	2	2.173	0.009				52.9
11[c]	2	1.834	0.0013	2	2.017	−0.0011	2	2.184	0.0046	1	2.896	0.0052	27.0
12[c]	1	1.782	−0.0002	4	1.989	0.0045	1	2.220	−0.0031	1	2.906	0.0054	13.7
13[c]	1	1.765	−0.0010	3	1.938	0.0024	2	2.169	0.0026	1	2.894	0.0036	13.0

[a] The $k^3\chi$ data were Flourier transformed over $k = 2.0-13$ Å^{-1}. Units are Å and Å^2 for r and $\Delta\sigma^2$, respectively. [b] Back-transform range: $r' = 0.9-2.1$ Å. [c] Back-transform range: $r' = 0.9-2.8$ Å.

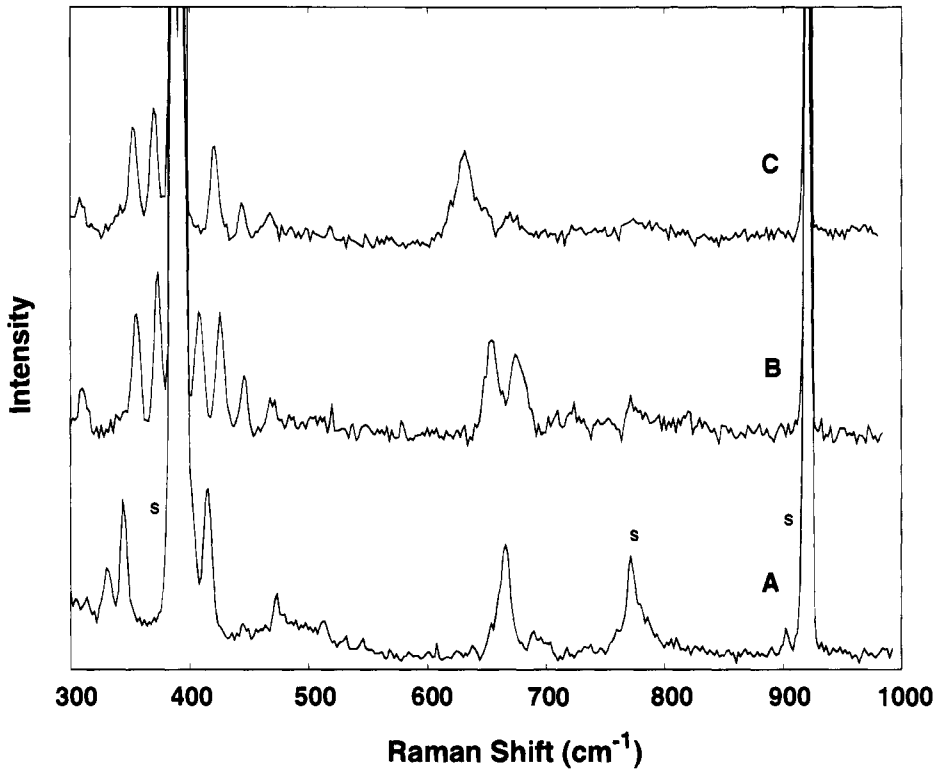

Figure 11. Resonance Raman spectra of **3a** (A), **3b** (B), and **3b** with added $H_2{}^{18}O$ (C) in CH_3CN. Spectra shown are the average of 5−10 scans obtained on frozen solutions at 77 K with laser excitation at 614 nm. Solvent features are labeled with S.

modes. However, a full assignment of the Raman features of **3** will require studies with isotopically labeled TPA ligands and a normal coordinate analysis.

EPR, Magnetization, and Mössbauer Studies. Figure 7 shows X-band EPR spectra of **3b** in acetonitrile (—) and as a solid (- - -). The 3.9 mM spectrum of Figure 7 exhibits sharp features at $g = 4.45$, 3.90, and 2.01 that can be assigned to the $M_S = \pm 1/2$ doublet of an $S = 3/2$ system described by

$$\mathbf{H}_e = D[\mathbf{S}_z^2 - S(S+1)/3 + (E/D)(\mathbf{S}_x^2 - \mathbf{S}_y^2)] + \beta\mathbf{S}\cdot\mathbf{g}_o\cdot\mathbf{H} \quad (1)$$

for $D \gg \beta H$, $E/D = 0.04$, $g_{ox} = 2.08$, $g_{oy} = 2.10$, and $g_{oz} = 2.01$. For $\lambda = E/D < 0.1$, the effective g values of the $\pm 1/2$ doublet can be computed from eq 1 to a good approximation[52] by

$$g_x = g_{ox}(2 - 3\lambda - (3/2)\lambda^2)$$
$$g_y = g_{oy}(2 + 3\lambda - (3/2)\lambda^2) \quad (2)$$
$$g_z = g_{oz}(1 - \lambda^2)$$

The resonances at $g_x = 3.90$ and $g_y = 4.45$ depend on the three unknowns g_{ox}, g_{oy}, and E/D; these unknowns therefore cannot be determined from EPR of the ground state alone (for example, $g_{ox} = 2.11$, $g_{oy} = 2.07$, and $E/D = 0.05$ would fit the data equally well). Since **3** is a dinuclear system for which the electronic structure is as yet not understood, the anisotropy of the intrinsic g_o values is not known. For the Mössbauer and magnetization studies described below, we have used the solution quoted for $E/D = 0.04$.

In a previous paper,[17] it was concluded that the green intermediate **3a** was a mononuclear rather than a dinuclear compound. This conclusion was based on EPR quantitations

(52) Münck, E.; Rhodes, H.; Orme-Johnson, W. H.; Davis, L. C.; Brill, W. J.; Shah, V. K. *Biochim. Biophys. Acta* **1975**, *400*, 32−53.

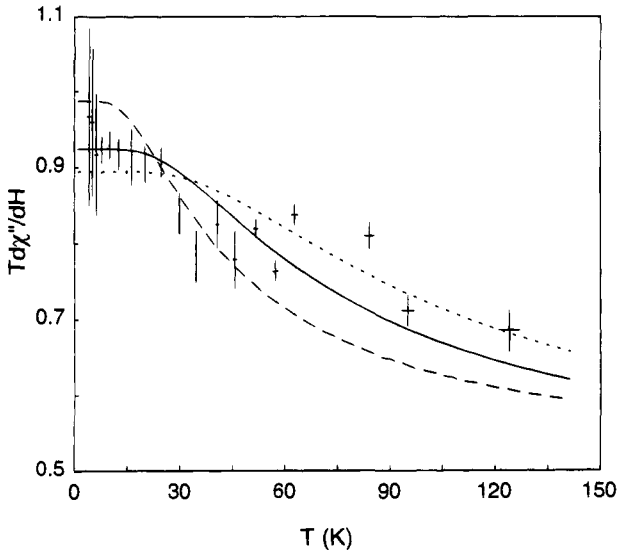

Figure 12. Temperature dependence of the solution EPR spectrum of Figure 7. The plot shows signal · T vs T, where the signal is measured as the area under the $g = 4.45$ feature. The theoretical curves are calculated for the ground doublet of an $S = {}^3/_2$ multiplet and $D = 20$ (- - -), 35 (—), and 50 cm^{-1} (• • •).

that indicated a spin concentration of 0.3 spin/Fe for samples that contained, according to Mössbauer spectroscopy, 30% of the Fe in a spectroscopic state characteristic of the green intermediate. Our recent studies indicate that the previous EPR quantitations were in error. The most significant error may have been introduced by quantitating the TPA complex against an $S = {}^3/_2$ Fe(EDTA)—NO complex, although problems with low-temperature transfers of these metastable samples seem to have contributed as well. Using Mössbauer spectroscopy to determine the fraction of Fe belonging to **3b**, we have recently obtained 0.75, 0.85, 1.00, and 1.25 spins/2Fe for four samples of **3b** dissolved in acetonitrile.[53] For these quantitations we have used Cu^{II}EDTA standards dissolved in water/glycerol (90:10 v/v) and corrected for the contraction and expansion of acetonitrile and water/glycerol, respectively. We have also confirmed that changes in the Q value of the cavity, due to solvent differences between the standard and the unknown, do not significantly affect the results. The values for the spin concentrations support the results obtained by mass spectrometry, SQUID magnetometry, and EXAFS, namely that **3** is a dinuclear complex.

The temperature dependence of the EPR signal is shown in Figure 12.[54] The value of signal · T decreases with increasing temperature due to the depopulation of the ground doublet. The theoretical curves in Figure 12 were calculated for $D = 20$, 35, and 50 cm^{-1}. From these curves we conclude that $D = 35 \pm 15$ cm^{-1}.

Figure 13 displays the results of magnetization studies of solid **3b**; the same solid material was studied with Mössbauer spectroscopy to yield the spectra of Figures 8 and 14. Besides establishing for the sample the fraction of Fe belonging to **3b**, the Mössbauer studies show the absence (<1%) of high-spin Fe^{III} impurities that could adversely affect the analysis of the magnetization data. Figure 13 shows curves reflecting es-

(53) The observed scatter in the spin concentrations is to a large extent attributable to handling of cold material and transfer of samples into EPR tubes. For example, the values 1.00 and 1.25 spins/2Fe were obtained for two samples prepared from the same batch of **3b**. These values were found to be reproducible for each sample and for quantitations performed on different days on the same sample.

(54) In some preparations of **3b**, we have observed a resonance at $g = 2.0$ with a width of ca. 10 mT. This signal was observed only at temperatures above 30 K. Its spin concentration at 70 K was approximately 3% of that obtained for **3b**. In one sample the signal was not observed at all. Given the low spin concentration of the signal and its variability between samples, it appears that it is not associated with **3b**.

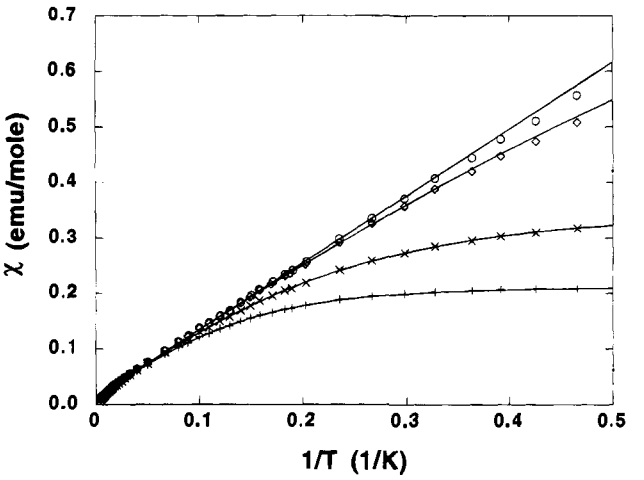

Figure 13. Temperature dependence of the magnetic susceptibility of **3b**. The experimental data were taken at magnetic fields of 0.1 (○), 1.0 (◇), 3.0 (×), and 5.0 (+) T. The solid lines represent the fitting for the $S = {}^3/_2$ system with $D = 40$ cm^{-1}, $E/D = 0.04$, $g = 2.1$, 2.1, 2.01.

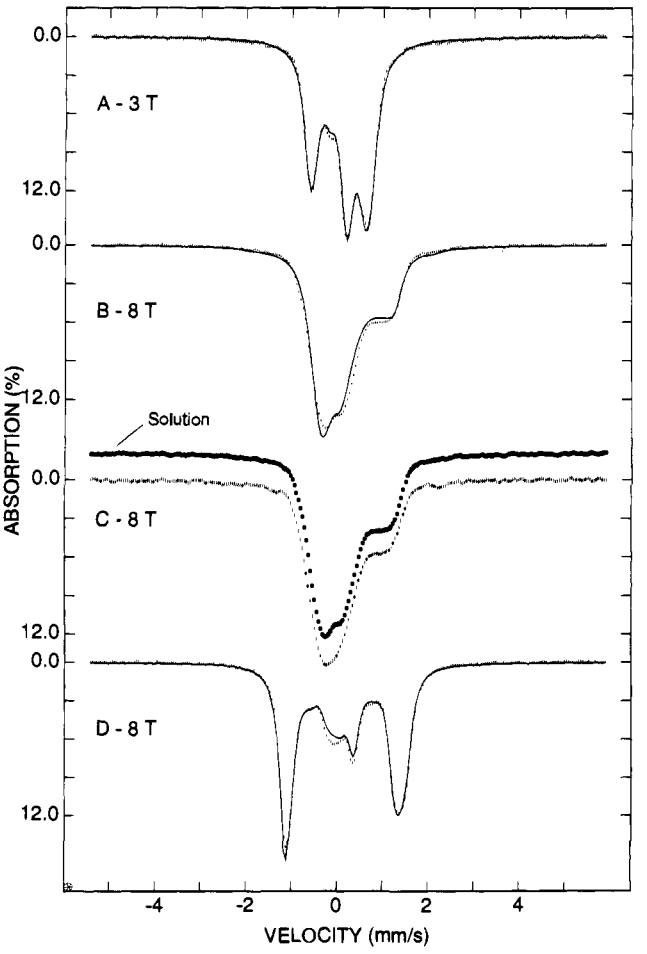

Figure 14. Mössbauer spectra of complex **3b** recorded in parallel applied magnetic fields as indicated: (A) solid at 1.5 K; (B) solid at 4.2 K; (C) solid at 4.2 K; (D) solid at 100 K. Part (C) shows a comparison of the spectra obtained in the solid and in frozen solution (solid circles). The solid lines drawn through the spectra of (A), (B), and (D) are theoretical spectra computed from eq 3 for $S = {}^3/_2$, $D = 30$ cm^{-1}, $E/D = 0.04$, $\Delta E_Q = 0.49$ mm/s, $\eta = 0.2$, $A_x = -7.8$ MHz, $A_y = -7.9$ MHz, $A_z = -6.5$ MHz, and $\delta = 0.14$ mm/s.

sentially the Zeeman splitting of the ground Kramers doublet of the $S = {}^3/_2$ system. We have fitted the data by assuming that the sample contains diamagnetic material and one $S = {}^3/_2$ species describable by eq 1 with values for $g_o = 2.1, 2.1, 2.01$ and $E/D = 0.04$ determined by EPR. This leaves the magnitude of D and the concentration of **3b** as free parameters.

The fits shown in Figure 13 afford 13 μmol of **3b**, in good agreement with the 13.9 μmol value for the amount of diiron cluster determined by iron analysis and corrected for the 10% diamagnetic Fe found by Mössbauer spectroscopy. Thus, the magnetization data also establish that **3** is a dinuclear complex. We have fitted the data of Figure 13 for a wide range of D values. The best fit was obtained for $D = 40$ cm^{-1}. However, while $D < 20$ and >60 cm^{-1} produced unacceptable fits, D values in the range 20 cm^{-1} $< D <$ 60 cm^{-1} cannot easily be dismissed if one would allow for minor undetected paramagnetic impurities or inadequacies of the Hamiltonian of eq 1.[55] The high-temperature data yield an effective moment of 3.9 μ_B/2Fe in good agreement with that computed for an $S = {}^3/_2$ system with $\mathbf{g_o}$ as determined by EPR.

As noted earlier, the Mössbauer spectrum of **3b** represents 90% of the sample and consists of a symmetric quadrupole doublet with Lorentzian lines of 0.27 mm/s, $\Delta E_Q = 0.49$ mm/s, and $\delta = 0.12$ mm/s (Figure 8). The narrow lines demonstrate that both Fe sites of **3b** have essentially identical environments. In fact, all Mössbauer spectra of **3b** could be analyzed by assuming identical sites. The remaining 10% of the sample belongs to a diamagnetic (μ-oxo)diiron(III) species whose spectral contributions can be simulated quite well for the entire range of applied fields and temperatures. The high-field spectra of **3b**, shown in Figure 14, were obtained by subtracting the theoretical spectra of this minority species from the raw data.

Before discussing the analysis of the low-temperature spectra of **3b**, a few comments are in order. Although **3** is a Kramers system that exhibits slow spin–lattice relaxation on the time scale of Mössbauer spectroscopy, the zero-field Mössbauer spectra of **3b** consist of quadrupole doublets down to 1.5 K. The lack of magnetic features in these spectra can be attributed to weak intermolecular spin–spin coupling. The asymmetry of the broadened quadrupole doublet of Figure 8B indicates that the relaxation rate is fast enough to cause the disappearance of resolved magnetic hyperfine interactions but not fast enough to produce at 4.2 K a doublet as sharp as that observed at 100 K (where the spin–lattice relaxation rate dominates). Spectra recorded at intermediate relaxation rates are the most difficult to analyze. However, the Mössbauer spectra are independent of relaxation under conditions for which only the "spin-down" level of the ground Kramers doublet is populated. Spectra shown in parts A and B in Figure 14 satisfy this condition.

The effects of spin–spin interactions are also apparent in acetonitrile solution for which we have observed pronounced broadening of the EPR signal of **3b** upon increasing the concentration from 0.1 to 3.9 mM. Using ^{57}Fe-enriched material, we have studied the Mössbauer spectra of **3a** and **3b** in acetonitrile solutions. All samples examined contained at least a fraction of molecules that experienced spin–spin interactions, even at concentrations as low as 0.4 mM of **3b**. As shown in Figure 14C, under conditions for which spin–spin interactions are suppressed by application of strong magnetic fields, the spectra of **3b** in acetonitrile are the same as those observed in the solid.

We have analyzed the Mössbauer spectra with the $S = {}^3/_2$ spin Hamiltonian

$$\mathbf{H} = \mathbf{H}_e + \mathbf{H}_{hf} \tag{3}$$

$$\mathbf{H}_{hf} = \mathbf{S}\cdot\mathbf{A}\cdot\mathbf{I} + (eQV_{zz}/12)[3\mathbf{I}_z^2 - I(I+1) + \eta(\mathbf{I}_x^2 - \mathbf{I}_y^2)] - g_n\beta_n\mathbf{H}\cdot\mathbf{I} \tag{4}$$

In eq 4, **A** is the magnetic hyperfine tensor describing the interactions of the ^{57}Fe nucleus with the electronic environment, while the second and third terms describe the quadrupole and nuclear Zeeman interactions, respectively. Because both Fe sites yield the same spectra, we do not have to sum over the two sites in eq 4.

As reported previously for **3a**, the magnetic hyperfine interactions of **3b** are unusually small. Furthermore, the A tensors of the two Fe sites have negative components. Thus, the internal magnetic field, $\mathbf{H}_{int} = -\langle\mathbf{S}\rangle\cdot\mathbf{A}/g_n\beta_n$, is negative for the "spin-down" level of the ground doublet; its magnitude along x and y is approximately 5.5 T. Hence, the effective field, $\mathbf{H}_{eff} = \mathbf{H}_{int} + \mathbf{H}$, acting on the nucleus is even smaller because the applied field opposes the internal field. The parameters listed in Table 3 are spectral simulations using eq 3 and assuming that the electronic spin fluctuates fast. Overall, the parameter set fits the data quite well. The minor mismatch in the center of the spectrum of Figure 14D is most likely due to thickness broadening which attenuates the more intense outer bands relative to inner features. Our simulations show that the features of the 4.2 K Mössbauer spectra are determined almost entirely by the properties of the $M_S = \pm{}^1/_2$ doublet. This implies that the $M_S = \pm{}^3/_2$ doublet is at an energy such that thermal population and mixing of the $\pm{}^1/_2$ levels with the $\pm{}^3/_2$ states by the applied field is negligible. Our simulations show that $D > +15$ cm^{-1}. These conclusions are in accord with the EPR and magnetization studies. The Mössbauer data are best fit with $D \sim 30$ cm^{-1}; however, for $D > 15$ cm^{-1}, the data are quite insensitive to the value of D.

Electronic Description of 3. The formula for **3** implies a complex that is *formally* $Fe^{III}Fe^{IV}$. That **3** is a high-valent species is indicated by the X-ray absorption K-edge energy of 7126 eV observed for **3b**, which is significantly higher than that of the starting complex **2b** (7123.3 eV). Furthermore, this high-valent species can be reduced by one electron. The addition of 1 equiv of ferrocene to **3b** causes its characteristic green color to disappear and converts it to a diiron(III) species with Mössbauer parameters (Table 3) similar but not identical to its precursor complex **2b**. Complex **3b** also exhibits a quasi-reversible cyclic voltammetric wave in CH_3CN at -40 °C with $E_{1/2} = 0.96$ V vs NHE ($\Delta E = 74$ mV), which we assign to the $[Fe_2O_2]^{3+/2+}$ couple (Figure 15). Similarly, **3a** exhibits a quasi-reversible wave at 1.05 V vs NHE. The lower potential of the 5-Me-TPA intermediate is consistent with its greater stability that presumably derives from the presence of the electron-donating methyl substitutents.

How can the electronic structure of **3** be described? Any description must take the following properties into account. (a) The complex is one oxidation equivalent above the diiron(III) state. (b) Its K-edge is ≈3 eV above that of its precursor (μ-oxo)diiron(III) complex. (c) The ground state has a system spin $S = {}^3/_2$ with a large zero-field splitting, namely $D \approx 35 \pm 15$ cm^{-1}, and g_o values of approximately $g_{ox} = g_{oy} = 2.1$ and g_{oz}

(55) We have good experimental data for the ground doublet. For the quoted values of $\mathbf{g_o}$ and for $E/D = 0.04$, the $M_S = \pm{}^3/_2$ doublet has effective g values of $g_x \approx g_y = 0.25$ and $g_z = 6.05$ and is therefore practically EPR silent. Given the observation that **3** has a large zero-field splitting, it is conceivable that quartic terms need to be added to eq 1. Moreover, since we do not yet understand the nature of the electronic ground state in terms of a spin coupling model, excited states of as yet unknown nature could influence the high-temperature magnetization data. However, it should be emphasized that our data are quite well described by the assumption of an isolated $S = {}^3/_2$ manifold.

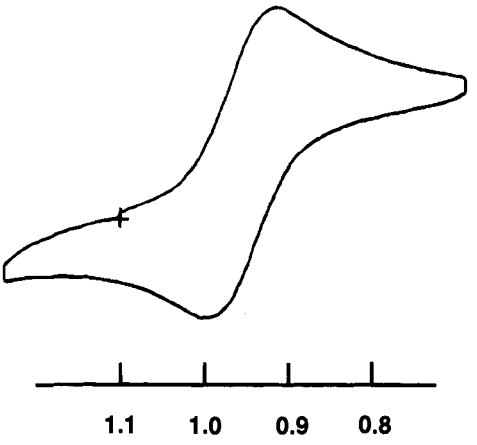

Figure 15. Cyclic voltammogram of **3b** in CH_3CN with 0.1 M $[Bu_4N][BF_4]$ at −40 °C. The potential was determined with ferrocene as the external standard.

= 2.01 (eq 1). (d) The two Fe sites are equivalent on the Mössbauer time scale at 1.5 K. (e) The iron sites have an isomer shift δ of 0.14 mm/s at 4.2 K, a small and temperature-independent ΔE_Q, and an unusually small and negative magnetic hyperfine field.

The iron site equivalence of **3** is reminiscent of two other diiron complexes, $[Fe_2(\mu\text{-}OH)_3(Me_3TACN)_2]^{2+}$ (**5**)[56] and [Fe(TPP)]$_2$N (**6**),[57] both of which are formally mixed-valence species, and reduced Fe_3S_4 clusters.[58] Extensive studies of the Mössbauer spectra of Fe_3S_4 clusters by Papaefthymiou and coworkers led to the recognition that the description of the magnetic properties of delocalized mixed-valence systems requires consideration of double exchange.[58] This concept, originally introduced by Zener,[59] found fruitful application for the analysis of the Mössbauer spectra of **5**, an $Fe^{II}Fe^{III}$ complex which exhibits equivalent iron sites in its 4.2 K Mössbauer spectrum with an isomer shift intermediate between high-spin Fe(II) and high-spin Fe(III) values.[56] For a mixed-valence compound, site equivalence can be explained by double exchange interactions which, as a consequence of resonance delocalization of the excess electron, can produce sites with identical A tensors, quadrupole interactions, and isomer shifts. For a mixed-valence pair, the relevant Hamiltonian yields the system energies

$$E = (J/2)S(S + 1) \pm B(S + 1/2) \qquad (5)$$

where S is the dimer spin and J and B are the coupling constants for Heisenberg ($H = J\mathbf{S}_1 \cdot \mathbf{S}_2$) and double exchange, respectively.[58] Wieghardt et al. determined $J \geq 235$ cm^{-1} and $B = 1300$ cm^{-1} for **5**,[56] showing that double exchange can be the dominating term in mixed valence systems. Thus, **5** is a Type III mixed-valence complex in the Robin−Day scheme with a ground state spin of $^9/_2$.

Complex **6** and related compounds $[Fe_2(Pc)_2N]$ (**6a**) and [(TPP)FeNFe(Pc)] (**6b**), like **3**, are one oxidizing equivalent above the diiron(III) state but, unlike **3**, have $S = {}^1/_2$ ground states.[57] Although the X-ray structure and physical properties of $Fe_2(TPP)_2N$ (**6**) were reported nearly two decades ago,[57a,b] the electronic structure of this compound is as yet not understood. The two Fe sites have $\delta = 0.18$ mm/s and $\Delta E_Q = 1.09$ mm/s; recent Mössbauer studies have shown that both Fe sites are indistinguishable and that the ^{57}Fe A tensors have axial symmetry (C. Achim, S.-J. Kang, R. G. Scheidt, and E. Münck, unpublished data). None of the parameters obtained thus far unambiguously identify the oxidation and spin state of the heme iron.

The observed iron site equivalence of **3** suggests that it may be described as a valence-delocalized $Fe^{III}Fe^{IV}$ pair or as a system consisting of two Fe^{III} sites coupled to a ligand radical. The coupled diiron(III)−radical model has been successfully applied to cluster **X** of ribonucleotide reductase.[12] In **X**, the high-spin ferric character of the iron sites is evident from their isomer shifts $\delta_1 = 0.55$ mm/s and $\delta_2 = 0.36$ mm/s.[60] These two iron sites are antiferromagnetically coupled to each other and further coupled to a radical to afford a ground state spin of $^1/_2$.[12] A similar description may be applied to **6**, **6a**, and **6b**, but the much smaller isomer shifts observed ($\delta = 0.18$, 0.06, and 0.11 mm/s, respectively)[57] favor a low-spin Fe^{III} assignment for these complexes, though intermediate spin Fe^{III} cannot be excluded presently. If the iron sites were indeed low spin, the $S = {}^1/_2$ system spin would derive from the antiferromagnetic coupling of two low-spin Fe^{III} centers with a nitrido radical. Since **3** has an isomer shift in the same range as **6**, **6a**, and **6b**, the iron centers may have low-spin Fe^{III} character. However, the $S = {}^3/_2$ system spin of **3** requires ferromagnetic coupling of two low-spin iron sites with a ligand radical; at present it is difficult to conceive of a bonding scheme that would give rise to such a ferromagnetic interaction.

The formulation of **3** as having two low-spin Fe^{III} centers is inconsistent with several of its properties. The ca. 3 eV edge shift observed in the XAS spectrum on going from **2b** to **3b** suggests an oxidation of the metal center(s) and not merely a change from high-spin to low-spin Fe^{III}. While a low-spin Fe^{III} configuration would be plausible for the indicated FeN_4O_2 coordination,[61] it seems difficult to explain the observed isotropy of the g_o values and the small A values with localized Fe^{III} sites, because low-spin Fe^{III} centers generally have very anisotropic g values and A tensors of sizable magnitude.[60b] Moreover, small and temperature-independent ΔE_Q values are exceedingly rare for low-spin Fe^{III}. Further, since $S = {}^1/_2$ multiplets do not have zero-file splittings, the large D value of the $S = {}^3/_2$ multiplet of **3** would have to be attributed to anisotropic exchange between the Fe^{III} sites. However, if we take a $D = 35$ cm^{-1} for **3**, interaction of the two iron(III) sites would have to produce an anisotropic exchange term of nearly 200 cm^{-1} in magnitude (see eq 4.49 and Table 4.4 of ref 62). We have recently observed anisotropic exchange of ca. 5 cm^{-1} for a cyanide-bridged Cu−heme complex containing a low-spin iron(III) ion;[63] anisotropic exchange of magnitude 200 cm^{-1} seems implausible to us.

(56) (a) Ding, X.-Q.; Bominar, E. L.; Bill, E.; Winkler, H.; Trautwein, A. X.; Drüeke, S.; Chaudhuri, P.; Wieghardt, K. *J. Chem. Phys.* **1990**, *92*, 178−186. (b) Drüeke, S.; Chaudhuri, P.; Pohl, K.; Wieghardt, K.; Ding, X.-Q.; Bill, E.; Sawaryn, A.; Trautwein, A. X.; Winkler, H.; Gurman, S. J. *J. Chem. Soc., Chem. Commun.* **1989**, 59−62.

(57) (a) Scheidt, W. R.; Summerville, D. A.; Cohen, I. A. *J. Am. Chem. Soc.* **1976**, *98*, 6623−6628. (b) Summerville, D. A.; Cohen, I. A. *J. Am. Chem. Soc.* **1976**, *98*, 1747−1752. (c) Kadish, K. M.; Bottomley, L. A.; Brace, J. G.; Winograd, N. *J. Am. Chem. Soc.* **1980**, *102*, 4341−4344. (d) Schick, G. A.; Bocian, D. F. *J. Am. Chem. Soc.* **1983**, *105*, 1830−1838. (e) Ercolani, C.; Hewage, S.; Heucher, R.; Rossi, G. *Inorg. Chem.*, **1993**, *32*, 2975−2977.

(58) Münck, E.; Papaefthymiou, V.; Surerus, K. K.; Girerd, J.-J. *ACS Symp. Ser.* **1988**, *372*, 302−325.

(59) Zener, C. *J. Phys. Rev.* **1951**, *82*, 403−405.

(60) (a) Greenwood, N. N.; Gibb, T. C. *Mössbauer Spectroscopy*; Chapman and Hall: London, 1971. (b) Rhynard, D.; Lang, G.; Spartalian, K.; Yonetani, T. *J. Chem. Phys.* **1979**, *71*, 3715−3721.

(61) Examples of low-spin Fe(III) complexes with N_4O_2 coordination include [Fe(sal$_2$trien)]NO_3 (Sinn, E.; Sim, G.; Dose, E. V.; Tweedle, M. F.; Wilson, L. J. *J. Am. Chem. Soc.* **1978**, *100*, 3375−3390) and [Fe(5-Me-TPA)acac]$(ClO_4)_2$ (Dong, Y., unpublished results).

(62) Bencini, A.; Gatteschi, D. *Electron Paramagnetic Resonance of Exchange Coupled Systems*; Springer-Verlag: Berlin, 1990.

Alternatively, **3** may be described as a valence-delocalized $Fe^{III}Fe^{IV}$ complex resulting from coupling a high-spin ($S_1 = 2$) Fe^{IV} and a high-spin ($S_2 = {}^5/_2$) Fe^{III} site or coupling a low-spin ($S_1 = 1$) Fe^{IV} and a low-spin ($S_2 = {}^1/_2$) Fe^{III} site. Such a mixed-valence description would explain the ca. 3 eV edge shift observed when **2b** is converted to **3b**, and the iron site equivalence would be achieved by invoking double exchange. In the absence of double exchange, a dinuclear complex containing a high-spin ($S_1 = 2$) Fe^{IV} and a high-spin ($S_2 = {}^5/_2$) Fe^{III} site would have a ground state of either $S = {}^1/_2$ or ${}^9/_2$. If double exchange is included, eq 5 predicts an $S = {}^3/_2$ ground state for $1.5 < B/J < 2.5$. While this model would explain the ground state spin and the equivalence of the two Fe sites, the small magnetic hyperfine interactions would be difficult to rationalize. Thus, for the $S = {}^3/_2$ state resulting for $1.5 < B/J < 2.5$, the observed A values would be related to the intrinsic a values by

$$A = [13a(Fe^{III}) + 2a(Fe^{IV})]/30 \qquad (6)$$

It can be seen that the observed A values would reflect essentially the a value of high-spin Fe^{III}. Using $a = -29$ MHz for Fe^{III} and $a = -20$ MHz for Fe^{IV},[64] we can estimate $A \approx -14$ MHz, which is twice the observed value $A_{iso} = (A_x + A_y + A_z)/3 = -7.4$ MHz. Moreover, the large zero-field splitting of **3** argues against this particular model. Using the formulas given by Bencini and Gatteschi,[62] the zero-field splitting of the $S = {}^3/_2$ multiplet is given by $D = -D(Fe^{IV}) - (4/15)D(Fe^{III})$. Since the D values of iron(III) sites with FeN_4O_2 coordination are typically ≈ 1 cm^{-1}, the large splitting of the $S = {}^3/_2$ multiplet would have to be contributed by the Fe^{IV} site. The high-spin Fe^{IV} ground configuration is complementary to high-spin Fe^{II}. For the latter, the large values of D result from excited orbital states at very low energies. Thermal population of these orbitals at temperatures below 200 K then will yield a temperature-dependent ΔE_Q. The requirement of a large D value but lack of a temperature dependence of ΔE_Q for **3** argues against the presence of a high-spin Fe^{IV} site for **3**.

The coupling of an $S = 1$ Fe^{IV} (range of reported isomer shifts: -0.2 to 0.2 mm/s)[65] and a low-spin Fe^{III} center by Heisenberg as well as double exchange can afford a valence-delocalized species that has the appropriate spin state ($S = {}^3/_2$), the iron site equivalence, and the proper isomer shifts. Moreover, since $S = 1$ Fe^{IV} complexes have generally very large zero-field splittings, the large D value of **3** could be attributed to the contribution of the Fe^{IV}.[65a,b] However, it is not yet clear to us whether the small A values and the small and temperature-independent ΔE_Q can be explained. To our knowledge, double exchange involving low-spin Fe^{III} and Fe^{IV} sites has not been treated in the literature. The problem is not trivially solved, because both Fe^{III} and Fe^{IV} have closely spaced t_{2g} orbitals in octahedral symmetry that are mixed considerably by spin–orbit interactions. This mixing could give rise to multiple pathways for double exchange, and without a detailed theoretical study it is not apparent to us how the local hyperfine interactions will be averaged in such a situation.

In the final analysis, the exchange coupling models considered above may be inadequate to describe the electronic structure reflected by the unusual Mössbauer parameters observed for **3**. The high oxidation level of **3** may significantly increase the covalency of the Fe–O bonds, and a molecular orbital description may thus be more appropriate. To this end, we have initiated *ab initio* density functional theory calculations on species **3a**.[66]

Perspective

Complex **3** represents the first well-characterized nonheme iron complex with a formal $Fe^{III}Fe^{IV}$ oxidation state.[67] It is also the only characterized high-valent species derived from the reaction of H_2O_2 and a (μ-oxo)diiron(III) complex, which makes **3** particularly relevant for the oxygen activation chemistry of RNR R2 and MMOH.[11-15] Complex **3** thus provides a synthetic precedent for comparison with the various transient oxidizing species that have been observed for RNR and MMO. Both **3** and RNR cluster **X** are 1 equiv above the diiron(III) oxidation state, but in **X** the iron centers are both in the high-spin iron(III) state and the oxidizing equivalent is essentially stored on a ligand radical.[12] The differences may arise from the distinct ligand environments in **3** (nitrogen-rich) and **X** (presumably oxygen-rich) and the lower symmetry of the R2 site. Such valence redistribution is also observed for heme peroxidase compounds **I** and corresponding models, the electronic descriptions of which span the range from Fe^V to Fe^{IV}–porphyrin radical to Fe^{IV}–nonligand radical.[18,68]

Intermediate **3** is also relevant to putative and observed high-valent intermediates of MMO. The formal $Fe^{III}Fe^{IV}$ oxidation state is represented in the Lipscomb mechanistic scheme as compound **R**,[14] the species derived from the one-electron reduction of compound **Q** by substrate and implicated by the formation of transient substrate radicals in the course of the oxidation reaction.[69] In the mechanism proposed by Feig and Lippard,[1b] an $Fe^{III}Fe^{IV}$ species or its resonance equivalent, an Fe^{III}–O$^{\bullet}$–Fe^{III} moiety, is proposed to derive from reduction of a (μ-peroxo)diiron(III) intermediate by conserved Cys 151[5a] (which has a position analogous to that of Tyr122 in RNR R2[4a]) as a means of activating the bound peroxide; a similar mechanism has recently been proposed by Klinman for dopamine β-hydroxylase.[70] However, there is presently no spectroscopic evidence for any such species analogous to **3** in the MMO catalytic scheme.

What is most intriguing in the comparison of **3** with MMO intermediates is the similarity of the Mössbauer parameters of **3** ($\delta = 0.14$ mm/s; $\Delta E_Q = 0.49$ mm/s) and compound **Q** ($\delta_1 = \delta_2 = 0.17$ mm/s and $\Delta E_{Q1} = \Delta E_{Q2} = 0.53$ mm/s for the MMOH from *Methylosinus trichosporium* OB3b; $\delta_1 = 0.21$ mm/s, $\Delta E_{Q1} = 0.68$ mm/s, $\delta_2 = 0.14$ mm/s, and $\Delta E_{Q2} = 0.55$ mm/s for the MMOH from *Methylococcus capsulatus* (Bath)).[13,15] However, in considering the similarities, one should keep in mind that compound **Q** has an oxidation level one electron more oxidized

(63) Kauffmann, K.; Scott, M. J.; Lee, S. C.; Day, E. P.; Holm, R. H.; Münck, E., unpublished results.

(64) Kostka, K. L.; Fox, B. G.; Hendrich, M. P.; Collins, T. J.; Rickard, C. E. F.; Wright, L. J.; Münck, E. *J. Am. Chem. Soc.* **1993**, *115*, 6746–6757.

(65) (a) Debrunner, P. G. In *Iron Porphyrins*; Lever, A. B. P., Gray, H. B., Eds.; VCH: New York, 1989; pp 137–234. (b) Collins, T. J.; Fox, B. G.; Hu, Z.; Kostka, K. L.; Münck, E.; Rickard, C. E. F.; Wright, L. J. *J. Am. Chem. Soc.* **1992**, *114*, 8724–8725. (c) Vogel, E.; Will, S.; Tilling, A. S.; Neumann, L.; Lex, J.; Bill, E.; Trautwein, A. X.; Wieghardt, K. *Angew. Chem., Int. Ed. Engl.* **1994**, *33*, 731–734.

(66) Ghosh, A.; Almlöf, J.; Que, L., Jr., work in progress.

(67) $[Fe_2O(salen)_2]X$ complexes have been reported by Wollman and Hendrickson, but the isomer shifts reported are not consistent with the proposed Fe(III)Fe(IV) formulation. Wollman, R. G.; Hendrickson, D. N. *Inorg. Chem.* **1977**, *16*, 723–733.

(68) (a) Poulos, T. L. *Adv. Inorg. Biochem.* **1987**, *7*, 1–36. (b) Yamaguchi, K.; Watanabe, Y.; Morishima, I. *J. Chem. Soc., Chem. Commun.* **1992**, *23*, 1721–1723. (c) Nanthakumar, A.; Goff, H. M. *J. Am. Chem. Soc.* **1990**, *112*, 4047–4049. (d) Ochsenbein, P.; Mandon, D.; Fisher, J.; Weiss, R.; Austin, R.; K., J.; Gold, A.; Temer, J.; Bill, E.; Müther, M.; Trautwein, A. X. *Angew. Chem., Int. Ed. Engl.* **1993**, *32*, 1437–1439.

(69) Priestley, N. D.; Floss, G. H.; Froland, W. A.; Lipscomb, J. D.; Williams, P. G.; Morimoto, H. *J. Am. Chem. Soc.* **1992**, *114*, 7561–7562.

(70) Tian, G.; Berry, J. A.; Klinman, J. P. *Biochemistry* **1994**, *33*, 226–234.

than **3**; moreover, the FeN_4O_2 coordination environment of the iron sites of **3** is compared with the (presumably) $FeNO_5$ environment of the iron site of compound **Q**. The coordination differences are particularly relevant in view of the fact that an $Fe^{III}N_4O_2$ complex may be low-spin[61] whereas an $Fe^{III}NO_5$ site is most likely high-spin. Thus, in relating the parameters of **3** to those of compound **Q**, we may be comparing not only different ligand environments but also different spin states of the local sites of the exchange-coupled structures. On the other hand, since the combination of ΔE_Q and δ values is unusual, the similaries may express some common features in the electronic structure that still need to be elaborated. With the recognition that **3** is a dinuclear species with the oxidation state of the Fe sites as yet unspecified, the question arises whether the assignment of **Q** to a diiron(IV) species should be reconsidered. The results of the current study, in our view, do not suggest a different interpretation of the electronic state of **Q**. The assignment of the Fe^{IV} state is based on the observation that a low-spin Fe^{III} state is unprecedented for an $FeNO_5$ coordination environment and that the low isomer shift (δ_{av} = 0.17 mm/s versus 0.53 mm/s for oxidized MMO), therefore, suggests considerable Fe^{IV} character.

Whatever its electronic structure, the existence of **3** emphasizes the notion that high-valent diiron species can be accessed in a nonheme ligand environment and, thus, **3** serves as a starting point for understanding the nature of related species observed for RNR and MMO.

Acknowledgment. We thank Professor J. D. Britton for his assistance and expertise with the structure determinations. This work was supported by the National Institutes of Health Grant Nos. GM-38767 (L.Q.) and GM-22701 (E.M.). H.F. thanks the Uehara Memorial Science Foundation for support of his stay at the University of Minnesota. EXAFS data were collected at the Stanford Synchrotron Radiation Laboratory (SSRL), the National Synchrotron Light Source (Brookhaven National Laboratory, Beamline X-9A), and the Cornell High Energy Synchrotron Source (CHESS, station C-2). SSRL is funded by the Department of Energy, Office of Basic Energy Sciences, and its Biotechnology Program is supported by the N.I.H. Division of Research Resources. Beamline X9A at the NSLS at BNL is supported by the N.I.H. (RR-01633). CHESS is supported by the N.S.F. (DMR-9311772).

Supplementary Material Available: Tables of the crystallographic experimental details, the atomic coordinates, thermal parameters, bond lengths, and bond angles for $[Fe_2O(TPA)_2(H_2O)(ClO_4)](ClO_4)_3$ and $[Fe_2O(5\text{-Et-TPA})_2(OH)(H_2O)](ClO_4)_3$ (39 pages). This material is contained in many libraries on microfiche, immediately follows this article in the microfilm version of the journal, can be ordered from the ACS, and can be downloaded from the Internet; see any current masthead page for ordering information and Internet access instructions.

JA9431014